ELECTROCHEMICAL SUPERCAPACITORS

ADVANCED MATERIALS AND METHODS FOR THE FABRICATION OF ELECTROCHEMICAL SUPERCAPACITORS

By

Jun Li, B. Sc.

A Thesis
Submitted to the School of Graduate Studies
in Partial Fulfillment of the Requirements
For the Degree
Master of Applied Science

McMaster University

MASTER OF APPLIED SCIENCE (2009) McMaster University
(Materials Science & Engineering) Hamilton, Ontario

TITLE: Advanced Materials and Methods for the Fabrication of Electrochemical Supercapacitors

AUTHOR: Jun Li, B. Sc., (Zhejiang University, P. R. China)

SUPERVISOR: Professor I. Zhitomirsky

NUMBER OF PAGES: X, 108

Abstract

Nanostructured manganese oxides in amorphous or various crystalline forms have been found to be promising electrode materials for electrochemical supercapacitors (ES). Manganese dioxide nanofibers with length ranged from 0.1 to 1 μm and a diameter of about 3-10 nm were prepared by a chemical precipitation method. Electrophoretic deposition (EPD) method and impregnation techniques have been developed to fabricate thin film and composite electrodes for ES. As-prepared nanofibers and electrodes were studied by transmission electron microscopy (TEM), scanning electron microscopy (SEM), energy dispersive spectroscopy (EDS), X-ray diffraction (XRD), thermogravimetric analysis (TGA) and differential thermal analysis (DTA). The capacitive behavior of electrodes was investigated by cyclic voltammetry (CV) and chronopotentiometry method using a three-electrode cell in the mild Na_2SO_4.

The composite electrodes fabricated by impregnation of manganese dioxide nanofibers and multi-walled carbon nanotubes (MWCNTs) into porous nickel foam and nickel plaque current collectors showed excellent capacitive performance with large material loading of 7-40 mg cm^{-2} in 0.1-0.5 M Na_2SO_4. MnO_2 nanofibers and MWCNTs can form a porous fibrous network, which is beneficial for the electrolyte access to the active materials. In addition, MWCNTs formed a secondary conductivity network within the porous nickel structures. The highest specific capacitance (SC) of

185 F g^{-1} was obtained at a scan rate of 2 mV s^{-1} in the 0.5 M Na_2SO_4 solutions. The effect of the electrolyte concentration, scan rate and active material composition on the capacitive behavior was discussed.

Obtained thin film and composite electrodes by EPD showed a capacitive behavior in the 0.1 M Na_2SO_4 aqueous solutions with a potential range of 0-1.0 V. The highest SC of 412 F g^{-1} was obtained for the thin film electrodes at a scan rate 2 mV s^{-1} in the 0.1 M Na_2SO_4. The SC decreased with increasing deposit mass and scan rate. It was found that the addition of MWCNTs can improve the capacitive performance of manganese dioxide electrodes with smaller equivalent series resistance (ESR). The mechanisms and kinetics of all the deposition methods were discussed.

Acknowledgement

First and foremost I offer my sincerest gratitude to my supervisor, Dr. Igor Zhitomirsky, who has supported me thoughout my thesis with his patience and knowledge. I attribute the level of my Masters degree to his encouragement and effort and without him this thesis, too, would not have been completed or written. One simply could not wish for a better or friendlier supervisor.

My appreciation is also extended to the SEM technician Steve Koprich, XRD technician Wen-He Gong, and DTA&TGA technician Frank Gibbs for their assistance in my research. Many thanks to all my groupmates in Dr. Igor Zhitomirsky's lab, Marco Cheong, Xin Pang, Feng Sun, Rong Ma, Yaohui Wang, Chao Shi, and Gideon Moses Jacob for their kind help and friendship.

The Department of Materials Science & Engineering has provided the support and equipment I have needed to complete my studies. I am very thankful for the financial support from the Natural Science and Engineering Research Council of Canada (NSERC).

Finally, I thank my parents for their love and encouragement throughout all my studies at McMaster University in Canada.

Table of Contents

List of Figures

Chapter 1 Introduction

With growing environmental concerns and increasing depletion of petroleum-based fuels, much effort has been concentrated on the development of alternative energy technologies. Supercapacitors have been widely researched due to their interesting characteristics in term of high power density, excellent reversibility and cycling stability. Generally, based on the charge storage mechanisms, supercapacitors can be categorized into two types of capacitors[1]: the electrochemical double-layer capacitors (EDLC) and pseudocapacitors. EDLC consist of high specific surface area materials and store energy in the electrical double layers. Pseudocapacitor materials exhibit several oxidation states and store energy not only in double layers, but also in reversible redox reactions occurring on or near the electrode surface. Compared to EDLC, the pseudocapacitors typically exhibit better capacitive behavior with higher SC. Among several types of materials studied for supercapacitors, various forms of carbon (carbon nanotubes, activated carbon, carbon fibers, etc.), conducting polymers (polyaniline, polypyrrole, polythiophene, etc.), and metal oxides (oxides of manganese, ruthenium, nickel, etc.) have received enormous interest.

The low cost and natural abundance of manganese dioxide, coupled with the good electrochemical performance (the theoretical SC ~1370 F g^{-1})[2] and environmental compatibility, has made it a very promising electrode material for supercapacitors. However, the poor electronic and ionic conductivity of manganese dioxide result in poor materials utilization. The SC of manganese oxide films reported in the literature[3-5] is in the range of 100-300 F g^{-1}, which is far from the theoretical SC. Much work has been done to further improve the electrochemical performance of manganese dioxide. There is an increasing interest to develop advanced composite electrode materials. Conductive additives, such as carbon black, are usually added to manganese dioxide in order to increase the electronic conductivity of the composite electrodes and improve power-energy characteristics of supercapacitors. The goal of this investigation was the development of nanostructured manganese dioxide and manganese-dioxide/carbon nanotubes composite electrodes for application in advanced supercapacitors.

Chapter 2 Literature Review

2.1 The development of the supercapacitor technology

Supercapacitors also called 'ultracapacitors' or 'electrochemical capacitors' is a new kind of energy storage and conversion device. Electrochemical capacitors have been known for many years. In 1957, the first patent has been developed by General Electric engineers[6] related to a capacitor containing high surface area carbon and aqueous electrolyte. It was believed that the energy was stored in the carbon pores. The capacitor exhibited 'exceptionally high capacitance', although the mechanism of charge storage was unknown at that time. However, General Electric did not immediately follow up on this work, and the modern versions of the devices were eventually developed by researchers at Standard Oil of Ohio in 1966[7]. They used organic electrolyte instead of aqueous electrolyte to achieve a larger operation voltage and achieved higher power and energy densities. But Standard Oil failed to commercialize their invention and licensed the technology to NEC, who finally marketed the results as 'supercapacitors' in 1978, to provide backup power for maintaining computer memory[8]. In 1975-1981 Conway developed the theories and principles for another type supercapacitor, also named pseudocapacitor. It depended on the fast and reversible redox reactions occurring on or near the electrode surface. Ruthenium oxide films were first employed to make electrodes of pseudocapacitors[9-11]. They showed ideal capacitive behavior with long cycling life and high reversibility. In 1990s, due to the potential applications in the hybrid electric vehicles, the research of supercapacitors became popular. A DOE supercapacitors development program was initiated and also the short and long terms goals were defined respectively[12].

Until now, four types of supercapacitors are developed[13]. Generation I supercapacitors having electrodes comprised of ruthenium oxide and an aqueous electrolyte were investigated extensively during the past 25 years but have never reached commercial scale production, primarily, because of cost issues[1]. Generation II products having identical carbon electrodes (symmetrical construction), but with a nonaqueous electrolyte, followed quickly to allow higher unit cell operating voltages as the Panasonic Goldcap™. The Generation II type supercapacitors provided a step-increase in energy density over earlier products due to the higher unit cell operating voltage. It is the most common type in use today. In 1997, the Russian Company ESMA[14] introduced the Generation III device with an asymmetric design in which one electrode has three to ten times the capacity of the other[15], resulting in over twice the energy storage capability of earlier designs. The ESMA capacitors used a NiOOH positive electrode with a high surface area carbon negative electrode in an aqueous potassium hydroxide electrolyte. The Generation IV devices have an asymmetric design and operate at a higher voltage with an organic electrolyte for higher energy storage capability. This design operates exactly like Generation III devices but with a nonaqueous electrolyte. Generation III and IV supercapacitors are clearly capacitive since they showed a sloping discharging and a behavior described by capacitor equations. These devices can have cycle lives that are many orders of magnitude greater than any battery and can deliver a power performance higher than most batteries.

In 2005, the supercapacitor market was between US $272 million and $400 million, depending on the source. It is rapidly growing, especially in the automotive sector[16]. The supercapacitors technology is experiencing increasingly broader use, replacing batteries in some cases, and in others complementing their performance. In a few situations supercapacitors have been an enabling technology. Today, some companies such as Maxwell Technologies, EPCOS, NEC, Panasonic, ELNA, ROKIN, and several others invest in electrochemical capacitor development. Supercapacitors will be challenges and opportunities for real-world applications in 21st century.

2.2 Principles of energy storage in supercapacitors

According to the different energy storage mechanisms, supercapacitors can be classified to EDLC and pseudocapacitors[1]. In this chapter, mechanisms of two types of supercapacitors will be discussed and the difference in principles of energy storage of batteries and supercapacitors will also be presented and compared.

2.2.1 Electrochemical double-layer capacitors

EDLC are usually constructed from two carbon-based electrodes, an electrolyte, and a separator. The energy storage in EDLC is a result of the separation of charges at the interface between the electronic conducting electrode and the ionic conducting electrolyte, which is in the similar way as conventional capacitors. There is no transfer of charges between electrode and electrolyte. The capacitance built at this interface is called the double layer capacitance. High surface area activated carbon is one of the best examples of a double layer capacitor material. The electrochemical processes for a double-layer capacitor can be written as[17]

Positive electrode

$$E_S + A^- \underset{Discharge}{\overset{Charge}{\rightleftharpoons}} E_S^+ // A^- + e^- \qquad (2\text{-}1)$$

Negative electrode

$$E_S + C^+ + e^- \underset{Discharge}{\overset{Charge}{\rightleftharpoons}} E_S^- // C^+ \qquad (2\text{-}2)$$

Overall reaction

$$E_S + E_S + C^+A^- \underset{Discharge}{\overset{Charge}{\rightleftharpoons}} E_S^+ // A^- + E_S^- // C^+ \qquad (2\text{-}3)$$

where E_s represents the carbon electrode surface, // represents the double layer where charges are accumulated on the two sides of the double layer, and C^+ and A^- represent the cation and the anion of the electrolyte, respectively. As shown in Equation 2-1 and Equation 2-2, during the charge, electrons are forward from the positive electrode to the negative electrode through the external power sources; at the same time, positive and negative ions are separated from the bulk electrolyte and moved to the electrode surfaces. During the discharge, electrons move from the negative electrode to the positive electrode through the load, and ions are released from the electrode surface and moved back into the bulk of the electrolyte. As shown in the overall reaction, the salt (C^+A^-) in the electrolyte is consumed during charge, so the electrolyte can be considered as an active material. During the charge and discharge, the charge density at the interface of the electrode changes, and the salt concentration and the conductivity of the electrolyte also changes.

The double layer capacitance can be expressed by the following formula similar to the conventional capacitors

$$C_{dl} = \varepsilon\varepsilon_0 A / d \tag{2-4}$$

Where ε is the dielectric constant of the electrical double-layer region, ε_0 is the permittivity of free space, A is the surface area of the electrode, and d is the thickness of electrical double-layer, depending on the size of the ions and the concentration of the electrolyte. The separation distance d is usually in angstrom range for EDLC while the separations for the conventional capacitors are in micro-meter range. The surface area A is much lager than the area of the electrodes in conventional capacitors, due to the high surface area of active materials used in EDLC. Consequently, the capacitance of EDLC is usually much higher than the capacitance of conventional capacitors[1].

Because there is no transfer of charges between electrolyte and electrode, there are no chemical or composition changes associated with charge/discharge cycling. For this reason, charge storage in EDLC is fast and highly reversible, which allows them to achieve very high cycling stabilities. It is reported that EDLC can achieve 500,000 cycles without significant degradation[8].

2.2.2 Pseudocapacitors

The energy storage mechanism of pseudocapacitors is much more complex than EDLC. In contrast to EDLC, pseudocapacitors store energy mainly depending on the fast and reversible faradaic reactions occurring on or near the electrode surface at the appropriate potentials[1], which gives the advantage of fast charge/discharge rate, high reversibility and long cycle life. It is the Faradaic reactions that distinguish pseudocapacitors from EDLC. It should be pointed out that the double-layer capacitance always coexists with the pseudocapacitance. However, the numbers of ions involved in the separation and accumulation is much lower than the quantity of protons exchanged between two electrodes. According to the research of Shukla et al.[18], the pseudocapacitors have a capacitance value 70 times higher than carbon EDLC for the same area. The most representative electrode materials for pseudocapacitors are transition metal oxides, such as RuO_2. The electrochemical reactions for RuO_2 electrodes can be expressed as[17]

Positive electrode

$$HRuO_2 \underset{Discharge}{\overset{Charge}{\rightleftharpoons}} H_{1-\delta}RuO_2 + \delta H^+ + \delta e^- \tag{2-5}$$

Negative electrode

$$HRuO_2 + \delta H^+ + \delta e^- \underset{Discharge}{\overset{Charge}{\rightleftharpoons}} H_{1+\delta}RuO_2 \tag{2-6}$$

Overall reaction

$$HRuO_2 + HRuO_2 \underset{Discharge}{\overset{Charge}{\rightleftharpoons}} H_{1-\delta}RuO_2 + H_{1+\delta}RuO_2 \qquad (2\text{-}7)$$

Where $0<\delta<1$

RuO_2 and H_2RuO_2 represent the positive and the negative electrodes at fully charged states, respectively. $HRuO_2$ represents electrodes which are at the fully discharged state[19]. As shown, the proton transfer from one electrode to another occurs across the separator during the charge and the discharge. At the same time, electrons transfer through the power source or the external load. The concentration of the electrolyte remains constant during the entire charge and discharge.

There are a lot of factors that can influence the capacitance performance of pseudocapacitors, including the particle size of active materials, the conductivity of active materials, surface area of electrodes, the porosity of electrodes, the nature of electrolyte, the design of cells and other factors.

2.2.3 Energy density and power density of supercapacitors

Energy density and power density are two main fundamental parameters for describing the performance of energy devices. Energy density describes the ability of energy storage, while power density describes how fast the energy can be released. Conventional capacitors, supercapacitors, batteries and fuel cells are typical energy storage and conversion devices. For supercapacitors, the energy density and power density can be calculated by:

$$W=1/2\ CU^2 \qquad (2\text{-}8)$$

$$P=U^2/4R \tag{2-9}$$

Where U is the operating voltage, C is the SC and R is ESR. As shown in Equation 2-8 and Equation 2-9, the operating potential is an important determinant of both the specific energy and the power of supercapacitors, which is usually dependant on electrolyte stability. As to ESR, it mostly depends on the conductivity of the active materials and the porosity of the electrodes and the design of the cell.

Figure 2-1 is a typical 'Ragone plot' describing the differences of power and energy densities between various energy and conversion devices.

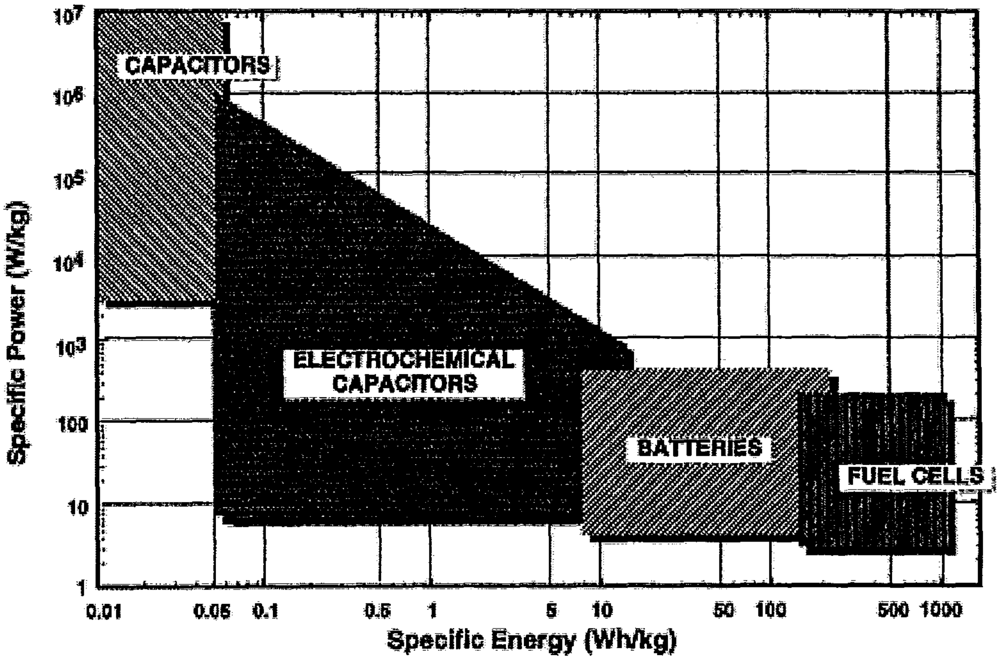

Figure 2-1 Sketch of Ragone plot for various energy storage and conversion devices. The indicated areas are rough guide lines[20]

As shown from the Figure 2-1, batteries and low temperature fuel cells are typical low power devices, whereas conventional capacitors may have a specific power of $>10^6$ watts per kg at very low specific energy. Supercapacitors fill the gap between batteries and conventional capacitors in terms of both specific energy and power, i.e. they have a specific power as high as conventional capacitors and a specific energy close to that of batteries. Therefore, supercapacitors may improve battery performance in terms of power density or may improve capacitor performance in terms of energy density when combined with the respective device.

2.2.4 Advantages of supercapacitor technology

The hybrid energy storage systems combing the supercapacitors and batteries are gaining great research interest. In such systems, supercapacitors can act as a power reserve to deliver peak power during a limited time. It is important to discuss the differences between these two types of devices and the advantages of supercapacitors, compared to the battery technology.

As discussed above, there are two different types of supercapacitors depending on the energy storage mechanism. Supercapacitors have higher specific power while the batteries have better performance in terms of specific energy. In order to understand the difference between batteries and electrochemical capacitors, it is important to analyze the different physical/chemical mechanisms of energy storage.

The batteries store energy in the bulk of chemical reactants capable of generating charge[21]. As a result, the batteries discharge rate and therefore power performance is then limited by the reaction kinetics as well as the mass transport, while such limitations do not apply to supercapacitors which only depend on the surface reactions[1], thereby allowing exceptionally high power density during both charge and discharge. Most batteries exhibit a relatively constant operating voltage because of the thermodynamics of the battery reactants. On the other hand, for a capacitor, its operating voltage changes linearly with time during constant current operation[22]. Furthermore, the highly reversible electrostatic charge storage mechanism in supercapacitors does not lead to any volume change like observed in batteries with electrochemical transformations of active masses. This volume change limits the cyclability of batteries generally to several hundred cycles, while supercapacitors show millions of full charge/discharge cycles. Supercapacitors exhibit charge/discharge efficiency of about 95%, because the energy losses related to heating during each cycle are relatively small. However, the energy losses in the batteries are much larger, making heat removal during operation more crucial and its extraction costs much higher.

From the comparison, it is clear that supercapacitors have shorter charge/discharge time, longer cycle life and higher cycle efficiency. As a result, supercapacitors will be very important for the future development of energy storage systems.

2.3 Applications of supercapacitors

With the emergence of new technologies and applications with challenging power requirements, there is increasing interest in supercapacitors, either as stand-alone energy-storage devices for high power needs or for hybrid supercapacitor-battery systems that simultaneously address both power and energy requirements.

2.3.1 Present applications

Generally, the applications of supercapacitors can be divided to three categories[12]: main power source, backup source and alternating power source. As the main power source, the supercapacitors can deliver one or several large current pulses of several milliseconds to several seconds duration. Afterwards the supercapacitors are recharged by a power supply of low power rating. As an example, cars with 'rechargeable motors' contain supercapacitors, which can be recharged from battery or some other power charger. The charge process takes about 10s and the power is supplied to the car for more than 10s. As for backup source, the supercapacitors are mostly served for memories, microcomputers, system boards and clocks. In these applications there is a main power source which normally supplies power to the load. The basic setup is the main power source (battery) paralleled with a supercapacitor. In case of power outages, due to disconnection or turn-off of the primary source, contact problems, a drop of the system voltage, the supercapacitor can supply energy. The supercapacitors are also used as alternating power sources, e.g. on a day-night basis. During the day the electric load is supplied by, e.g. solar cells, which also recharge the supercapacitors .During the night the power is delivered by supercapacitors. For example, in a solar watch, after being completely charged, the supercapacitor may feed the watch for several days. The watch does not need any battery replacement during its lifetime.

2.3.2 Upcoming applications

The supercapacitors bridge the critical performance gap between the high power density offered by conventional capacitors and the high energy density of batteries. Thus, with the help of supercapacitors, the power density of batteries and energy density of capacitor may improve a lot. Perhaps the most visible technologies that will be impacted by supercapacitors are hybrid-power systems, where significant increases in energy efficiency can be achieved through the recovery of energy normally wasted during braking, thanks to the rapid charge-discharge response of supercapacitors. Such waste energy harvesting will become increasingly important and popular in industrial equipment like cranes, fork-lifts, and elevators, as well as in many types of vehicles including automobiles, trucks, and buses[23]. All have great potentials for improved energy efficiency.

2.4 Materials for supercapacitors

Supercapacitors can be made from a variety of materials whose selection depends on the type of capacitance to be utilized, as shown in Figure 2-2.

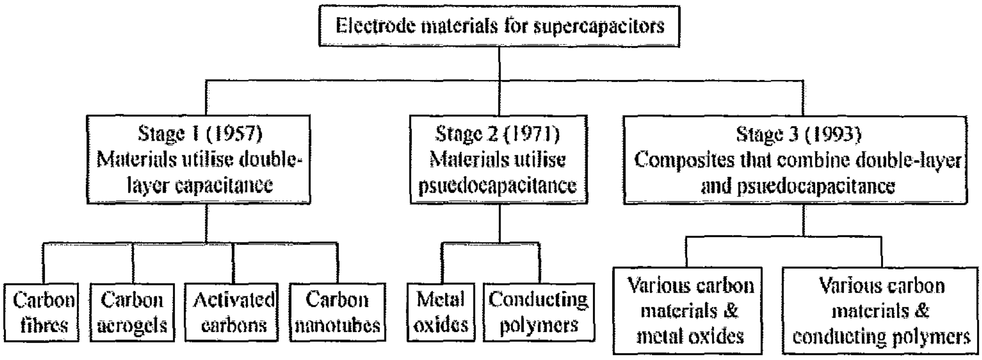

Figure 2-2 Taxonomy of the supercapacitor materials[24]

Carbon in its dispersed and conducting form is the most widely used commercial material for supercapacitors. Metal oxides such as ruthenium, cobalt, nickel, and manganese oxides are a family of materials used in supercapacitor applications. Conducting polymers are the third group of candidate materials for supercapacitors. Aside from the three categories of pure materials, there is a new tendency to synthesize composite materials combining two or more pure materials for supercapacitors. The very interesting direction is to combine carbon nanotubes with either metal oxides or conducting polymers.

2.4.1 Carbon materials

Carbon due to different allotropes, various microtextures, a rich variety of dimensionality from 0 to 3D and ability for existence under different forms represents a very wide range of materials for supercapacitor applications[25]. They have a unique combination of chemical and physical properties, namely: high conductivity, high surface area range, good corrosion resistance, high temperature stability, controlled pore structure, processability, compatibility in composite materials and relatively low cost[26]. They can be used as conductive additives, active materials, substrates for current leads in supercapacitors.

2.4.1.1 Carbon nanotubes (CNTs)

2.4.1.1.1 The fundamental knowledge of CNTs

CNT is another form of carbon first reported by Iijima in 1991 when he discovered MWCNTs in carbon- soot made by an arc-discharge method[27]. About two years later, he made the observation of single-walled nanotubes (SWCNTs)[28]. From then on, CNTs have captured the attention of researchers worldwide.

CNTs can be conceptualized as seamless hollow tubes rolled up from two-dimensional graphene sheets with diameters in the nanometer range and lengths usually on the micron scale[29]. Depending on the number of tube walls, CNTs can be classified into single-walled carbon nanotubes (SWCNTs) and MWCNTs. SWNTs are usually 1-2 nm in diameter and tens of microns in length. The structural characteristics of an SWCNT, namely its diameter and chirality, are usually described by a pair of indices (n,m). MWCNTs are made up of coaxial cylindrical carbon layers with an interlayer distance of 0.34 nm[27] and a diameter typically on the order of 10-20 nm.

CNTs are unique nanostructures that display the desirable properties of any other known materials. They have amazing electronic and mechanical properties which lead to high strength and conductivity. Experimental and theoretical results have shown an elastic modulus of greater than 1 TPa (that of a diamond is 1.2 TPa) and have reported strengths 10–100 times higher than the strongest steel at a fraction of the weight[30]. Also, the theoretical and experimental results show superior electrical properties of CNTs. They can produce electric current carrying capacity 1000 times higher than copper wires[31].

CNTs with their unique properties are leading to many promising applications. They can be used in the field of reinforcements in composites, sensors and probes, energy storage, electrochemical devices, nanometer sized electronics and so on.

Various methods have been explored to synthesize CNTs. The first method for the synthesis of MWNTs was through arc growth[28]. However, the most attractive method commercially used is condensation–vaporization method while the laser ablation method is known to produce carbon nanotubes with the highest quality and high purity of single walls[32].

2.4.1.1.2 Applications of CNTs in supercapacitors

The high surface-volume ratio, electric conductivity and mechanical stability make CNTs as the ideal material for supercapacitors. The presence of pores in electrodes based on CNTs due to the central canal and entanglement enables easy access of ions from electrolyte. CNTs naturally show capacitive behavior in their pure form. Figure 2-3 is the typical CVs and charge/discharge curves of CNTs.

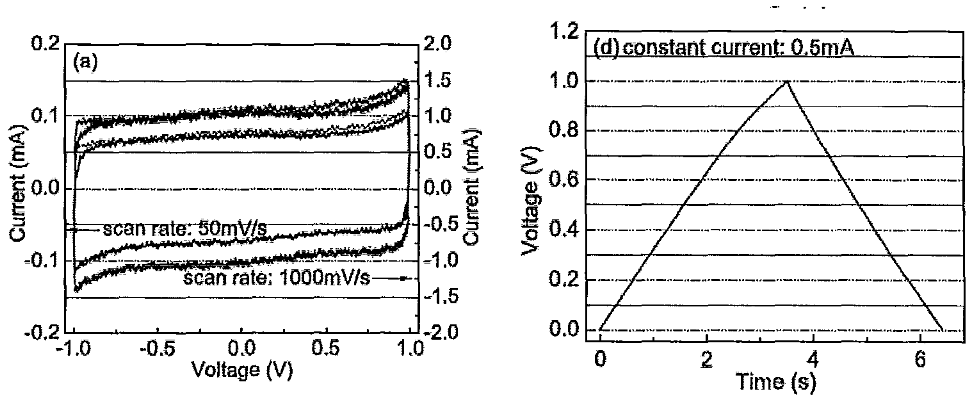

Figure 2-3 CVs and chronopotentiometry data of the nanotubes thin film supercapacitor[33]

The CVs present nearly rectangular shape, even at a very high scan rate, a clear proof of well developed capacitance properties. As can be seen, there is no IR drop in the discharge curve, reflecting the high conductivity of CNTs.

For electrodes built from MWCNTs, SC in a range of 4–135 F g^{-1} was found[34, 35]. For SWCNTs a maximum SC of 180 F g^{-1} and a measured power density of 20 kW kg^{-1} at the energy density of 7 Wh kg^{-1} in KOH electrolyte is reported[36]. B.J. Yoon *et al.*[37] fabricated CNTs-based electrodes by direct synthesis of CNTs on the bulk nickel substrates, by means of plasma enhanced chemical vapor deposition of methane and hydrogen. Rectangular CV shapes even at a scan rate of 1000 mV s^{-1} have been obtained. The SC was 38.7 F g^{-1}. Through surface treatment with ammonia plasma, higher value up to 207.3 F g^{-1} was reached.

The SC of CNTs can be increased by the attachment of functional group on the surface. Frackowiak et al.[38] successfully attached OH functional groups to the CNTs and demonstrated improved SC. Kim et al.[39] showed that the introduction of surface carboxyl groups created 3.2 times large SC due to the increased hydrophilicity of MWCNTs in an aqueous electrolyte. In contrast, the introduction of alkyl groups resulted in significantly lower SC due to the increased hydrophilicity of MWCNTs. However, the hydrophilicity of MWCNTs by aggressive oxidizing agent can damage the surface structure and decrease the conductivity of MWCNTs. A balance between hydrophilicity and conductivity is required.

CNTs can be also used in conjunction with other electrochemically active materials in the form of composite materials in supercapacitors. The open mesoporous network formed by the entanglement of CNTs allows the ions to diffuse easily to the active surface of the composite components. The exceptional conducting property of CNTs is essential to lower the ESR and consequently increase the power of the device. Moreover, since the nanotubular materials are characterized by a high resiliency, the composite electrodes can easily adapt to the volumetric changes during charge and discharge that improves drastically the cycling performance[40].

The addition of CNTs to activated carbon, instead of acetylene black or graphite powder for polarizable electrodes resulted in lower ESR and higher SC[41]. Addition of CNTs in manganese oxide electrode can increase the SC from 233 to 415 F g^{-1} and enhance the cycle stability of electrodes[42]. The SWCNTs/polypyrrole nanocomposite electrode showed much higher SC than pure polypyrrole or SWCNTs[43]. Supercapacitor electrodes based on CNTs/polyaniline nanocomposite, prepared by coating polyaniline on the surface of the CNTs, exhibited high SC of 201 F g^{-1}, in comparison with a value of 52 F g^{-1} for CNTs[44].

2.4.1.2 Other carbon materials

Among carbon materials, activated carbons are especially attractive as electrodes for EDLC from the economical point of view. Activated carbons are characterized by extremely large BET surface areas[26], which range from 500 to ~3000 $m^2\,g^{-1}$. With high surface areas, activated carbons show a good capacitive behavior and are widely used as an active material for negative electrodes in supercapacitors. Usually, the SC of activated carbons ranges from 100 to 200 F g^{-1} in aqueous medium, and from 50 to 150 F g^{-1} in organic medium[40]. The larger values in aqueous electrolyte are essentially justified by a smaller size of solvated ions and a higher dielectric constant than in organic media. Figure 2-4 is typical CVs of activated carbon in three different electrolytes.

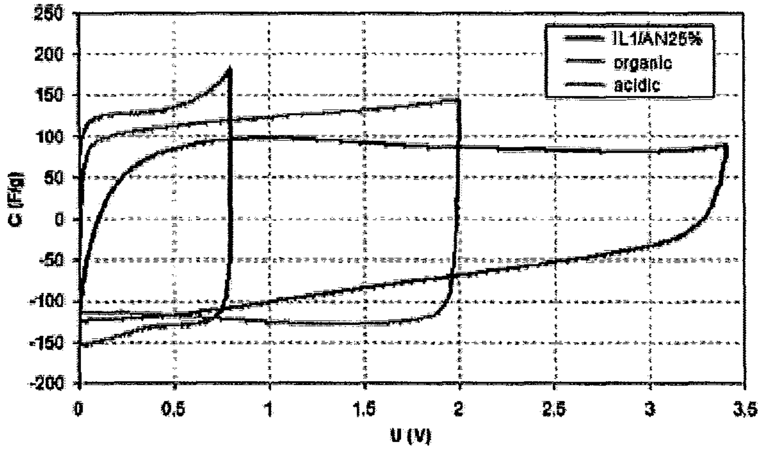

Figure 2-4 CVs of activated carbon electrode in three electrolytic media[45]

Activated carbons have all three types of pores classified by IUPAC[46]: micropores (diameters less than 2nm), mesopores (diameters between 2 and 50nm) and macropores (diameters greater than 50nm), which contribute to the high surface areas of activated carbons. However, not all pores are electrochemically accessible. If the size of the electrolyte ions is larger than the pores, it will result in the restriction of the movement of electrolyte. Eventually, there will be a limitation on the ability of the electrolyte to form a double layer. The surface area arising from pores in this size range would not contribute to the double layer capacitance. Moreover, as Frackowiak et al.[25] mentioned the high surface area and porosity can result in a poor conductivity, which limits the maximum power density of the supercapacitors.

In the supercapacitors based on activated carbon, the high porosity of activated carbon will also create the distributed electrolyte resistance, which restricts the rate of charge and discharge[26]. At low charge rate, electrolyte ions have time to penetrate into the depth of the pores and additional surface area is accessed, while electrolyte becomes poorer and less surface area is accessed at high charge rate.

Carbon blacks are another kind of attractive materials for supercapacitors, which usually have higher conductivity than activated carbon. The conductivity of carbon blacks is typically in the range 0.1 to 100 $(\Omega\,\mathrm{cm})^{-1}$ and is influenced by the relative ability of electrons to jump the gap between closely-spaced aggregates and by graphitic conduction via touching aggregates[47]. They can be used as conductive additives in batteries and supercapacitors to improve the conductivity of the electrodes. The loading of the carbon black is very critical. At low loadings, the inter-aggregate gap is too large for carbon blacks to influence the conductivity of composites. As the loading is increased, a percolation threshold is reached whereby the conductivity increases up to a limiting value[26].

2.4.2 Transition metal oxides

Besides carbon, transition metal oxides (ruthenium oxide, nickel oxide, manganese oxide, and cobalt oxide) are important materials for supercapacitors, which are being extensively studied due to their superior pseudocapacitive behavior.

2.4.2.1 Ruthenium oxide

Ruthenium oxide (hydrous or anhydrous) as a capacitive material has been widely studied since ruthenium dioxide was first reported as a new electrode material in 1971[10]. Ruthenium oxide which combines the metallic type conductivity and excellent reversible redox reactions in aqueous media together makes itself an excellent electrode material for pseudocapacitors. The redox reactions of ruthenium oxide not only occur at the electrode/electrolyte interface but also inside the bulk of the material[48]. Ruthenium oxide gives relatively constant and appreciable capacitance over a 1.0 V range[10] with SC ranging from 600 to 1000 F g^{-1} depending on the preparation procedure, measurement conditions, use of support, etc.[49] The high SC with low resistance and large operating potential resulted in very high specific power. Another advantage of ruthenium oxide is the ultra high stability or long cycle life that can be charged up to 10^5 times with little degradation[24]. Figure 2-5 is a typical CV of $RuO_2 \cdot xH_2O$, which shows ideal charge/discharge behavior in 0.5 M H_2SO_4 at scan rate 2 mV s^{-1}. However, the only problem related to $RuO_2 \cdot xH_2O$ is too expensive to be commercially attractive, thereby limiting its use as an electrode material of supercapacitors, which has stimulated a search for alternative electrode materials.

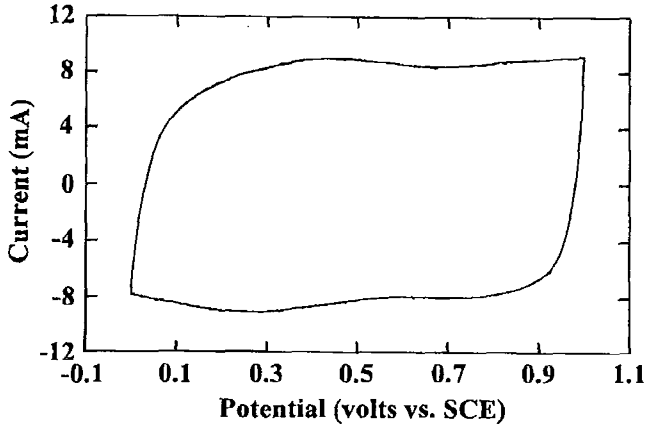

Figure 2-5 CV of ruthenium oxide electrode[48]

2.4.2.2 Manganese dioxide

Manganese dioxide is one of the potential candidates for use as electrode materials in pseudocapacitors. The first study reporting the capacitive behavior of manganese dioxide was published in 1999 by Lee and Goodenough[50]. They prepared α-MnO_2 with the BET surface area of 303 $m^2 g^{-1}$ by a chemical precipitation method and the powder was then rolled into a thin sheet. The measured SC of ~200 F g^{-1} was obtained and remained unchanged for 100 cycles in 2 M KCl electrolyte solution. The film showed ideal rectangular shape of CV and almost linear charge/discharge behavior

(Figure 2-6), which indicated a very good capacitive behavior. The manganese dioxide electrodes could work in a large potential window range from -0.2 to 1V in the mild electrolyte, which indicated a high energy density and power density according to the Equation 2-8 and Equation 2-9.

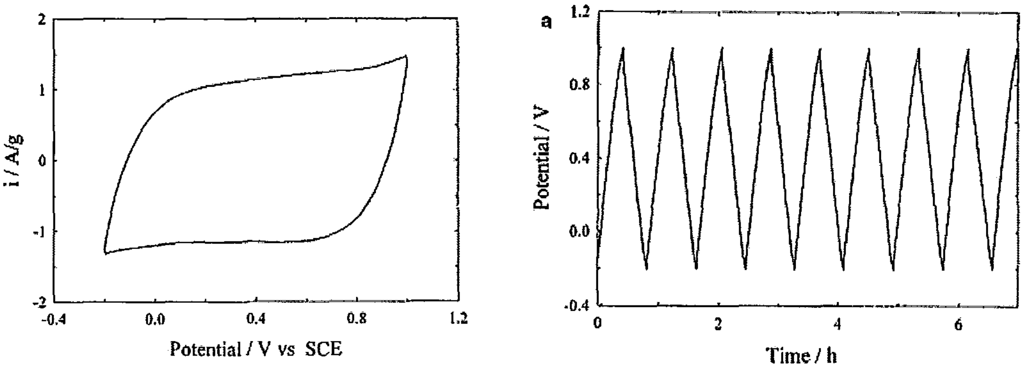

Figure 2-6 CV and chronopotentiometry data of manganese dioxide electrode[50]

Manganese dioxide as the active material for supercapacitors has received worldwide research interest due to the excellent capacitive behavior, low cost, natural abundance and environmental compatibility. A lot of papers were published since 1999. Pang et al.[51, 52] reported electrodeposited thin MnO_2 films (~4 μg cm^{-2}) with SC as high as ~700 F g^{-1} in a potential window of 0-0.9 V. Toupin et al.[53] achieved a very high SC of 1380 F g^{-1} for MnO_2 electrode, which is close to the theoretical value of 1370 F g^{-1} [2] expected for a redox process involving one electron per manganese atom. However, the SC of MnO_2 mostly reported in the literatures is in the range between 100 and 300 F g^{-1} [3-5].

The charge storage mechanism of manganese dioxide is believed to be predominantly due to pseudocapacitance, which is attributed to reversible redox transitions involving exchange of protons and /or cations with the electrolyte[51-53]. It can be expressed as:

$$MnO_\alpha(OH)_\beta + \delta H^+ + \delta e^- \leftrightarrow MnO_{\alpha-\delta}(OH)_{\beta+\delta} \qquad (2\text{-}10)$$

Where $MnO_\alpha(OH)_\beta$ and $MnO_{\alpha-\delta}(OH)_{\beta+\delta}$ indicate $MnO_2{\cdot}nH_2O$ at high and low oxidation states, respectively.

The disadvantage of manganese dioxide is its poor conductivity resulting in low material utilization and reactivity, which prevent itself from the ideal active material for supercapacitors. The charge/discharge only involved the surface atoms of the MnO_2 or a very thin layer. Only a limited fraction of the MnO_2 is electrochemically active. Toupin et al.[3] suggested that the protonic diffusion in the bulk of the MnO_2 compound might not be as fast as in the case of RuO_2. This might be the reasons for the reported SC of MnO_2 is far from the theoretical value.

Recently, the MnO_2/CNTs composite as an electrode material for supercapacitors attracted great attentions[42, 54, 55]. As discussed above, the addition of CNTs can bring the mesoporous network formed by the entanglement of CNTs and the exceptional conducting property, which will make MnO_2 electrodes more porous and also enhance the conductivity of MnO_2, thereby increasing the utilization of MnO_2 in the electrodes. The MnO_2/CNTs nanocomposite represents an important breakthrough for developing a new generation of supercapacitors.

2.4.2.3 Other metal oxides

Nickel oxide with low cost is another promising electrode material for pseudocapacitors. Liu et al.[56] developed an electrochemical pseudocapacitor using porous films of NiO_x prepared by the sol-gel technique. The SC of single NiO_x electrode was in the range from 200 to 256 F g^{-1}. Srinivasan et al.[57] used an electrochemical precipitation technique followed by heat-treatment to make NiO_x electrodes and the SC is ~240 F g^{-1}. The charge storage mechanism of NiO_x was studied and suggested to be[57, 58]:

$$NiO + OH^- \leftrightarrow NiOOH + e^- \qquad (2\text{-}11)$$

Figure 2-7 shows typical CVs of NiO_x. Compared to MnO_2 and RuO_2, the CV shape of NiO_x is asymmetrical, which results in the different charge/discharge behavior, and the range of the operating window is much smaller (0.5V), which reduces the power density and energy density of pseudocapacitors.

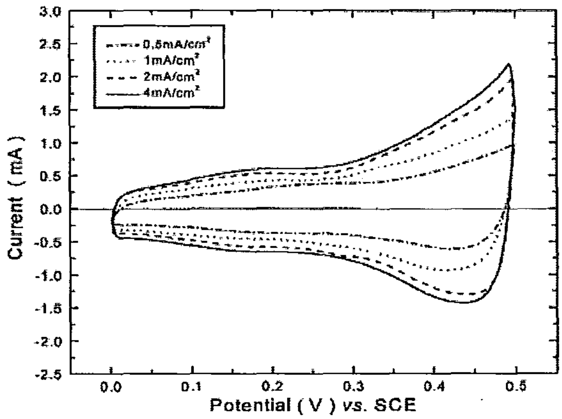

Figure 2-7 CVs of electrochemically deposited NiO_x electrodes[58]

Some other metal oxides with low cost have also been synthesized and tested for pseudocapacitor applications, e.g. cobalt oxide[59], iron oxide[60], tin oxide[61], vanadium oxide[62]. However, their SC and potential window are not comparable with RuO_2.

2.4.3 Conducting polymers

Conducting polymers have been considered as a promising group of materials for realization of high performance supercapacitors, due to their high electrical conductivity, fast charge/discharge processes, large pseudocapacitance and relatively low cost. The charge-discharge processes of conducting polymer-based electrodes are related to reversible faradic reactions known as n- and p- doping/undoping. Contrarily to double-layer activated carbons where only the surface is used for charge accumulation, in the case of conducting polymer, the total mass and volume is involved in charge storage[63], thereby obtaining higher capacitance value than activated carbons. The most commonly used conducting polymers include polyaniline (PANI), polypyrrole (PPy) and poly-[3,4-ethylenedioxythiophene] (PEDOT). They can easily reach high SC values, which are comparable with RuO_2, e.g. 775 F g^{-1} for PANI[64], 480 F g^{-1} for PPy[65] and 210 F g^{-1} for PEDOT[66], when the electrochemical investigation is performed in a three electrode cell using a thin film. It will be a very promising configuration in terms of charge storage capacity and cell voltage that an n-doped polymer and a p-doped polymer are used as negative and positive electrodes, respectively.

The main drawback of conducting polymers application as supercapacitor electrodes is connected with their poor mechanical stability during cycling due to volumetric changes during the doping/undoping processes[63]. They will undergo mechanical changes (swelling, shrinkage, cracks or breaking) that in consequence gradually aggravate their conducting properties. Additionally, the electrochemical activity of each conducting polymer is strictly determined by its working potential range and limited by an isolating state and/or polymer degradation caused by overoxidation.

It is well known that CNTs have an excellent mechanical property. Hence, the composite of CNTs and conducting polymer will be very interesting and attractive. The CNTs preserve the conducting polymer materials from mechanical changes during long cycling. E. Frackowiak et al.[63] conducted a research on conducting polymers/CNTs composites, which showed a much better cycle ability of conducting polymers/CNTs composite electrodes than conducting polymer electrode.

2.5 Electrolytes

The nature of electrolytes plays a very important role in the electrochemical characteristics of supercapacitors. The resistance of electrolytes can limit power density of supercapacitor cells, while their operating voltage, restricted by the breakdown potential of the electrolyte, can limit the energy density.

Generally, there are mainly two types of electrolytes used in supercapacitor technology: aqueous electrolytes and organic electrolytes. Aqueous electrolytes limit the unit cell voltage of the supercapacitor to typical 1V due to the thermodynamic electrochemical window of water (1.23V)[1], while organic electrolytes allow for a unit cell voltage above 2V. According to Equation 2-8 the square of the operating voltage determines the maximum stored energy. The low operating voltage of aqueous electrolyte will result in a low energy density compared with organic electrolytes. The disadvantage of organic electrolytes is the much higher specific resistance, which can reduce the maximum power density. Compared to a concentrated aqueous electrolyte the resistance increases by a factor of at least 20, typically by a factor of 50[20]. The relatively low conductivity of organic electrolytes results in low capacitance behavior of supercapacitors. In addition, organic electrolytes require a very stringent purification and drying processes during the production. If the electrolyte is not totally purified and dried, H_2 and O_2 may form on charge and subsequent recombination reactions, which leads to self-discharge. Usually, the cost of organic electrolytes is much higher than suitable aqueous electrolytes.

For aqueous electrolytes, the acid and alkaline electrolytes are mostly used in supercapacitors due to the advantageously high conductivities and the special mechanism of proton transport. The proton has the highest mobility in an aqueous electrolyte, and its small size allows it to chemisorb to a single oxide ion. In order to achieve a high conductivity to minimize the ESR and avoid the electrolyte depletion problems during charge, a high concentration of electrolytes is required. RuO_2 electrodes usually use concentrated H_2SO_4 as electrolytes[9, 10, 48, 49]. However, a strong acid medium is environmentally harmful and the number of oxides having appropriate redox energies that are stable in a strong acid solution is extremely limited. It is better to develop the mild electrolytes which are harmless to environment and much less corrosive to the electrodes. Lee and Goodenough[50] explore the use of a mild KCl aqueous electrolyte in MnO_2 based supercapacitors. Na_2SO_4 is another widely used electrolyte in the research field of supercapacitors[51-54].

As to organic electrolytes, practically, they most often based on acetonitrile or propylene carbonate as solvents allow to operate a supercapacitor to up to 2.3V. The solubility of the salts in the organic solvents is relatively low. If the electrolyte reservoir is too small compared to the large surface of electrodes, the performance of the supercapacitor is reduced. Consequently, it is very important to find proper salts with a good solubility in organic solvents. Tetraethyl ammonium salts have been preferred electrolytes due to good solubility and moderately good conductivity in organic solvents. For example, TEABF4 (tetraethyl ammonium tetrafluoroborate) dissolved in acetonitrile can allow supercapacitors to be charged/discharged up to 2.0V[45]. Nowadays, most of the presently available supercapacitors use organic electrolytes.

A further increase of supercapacitor voltage range can be achieved using ionic liquids, which are characterized by definitively higher decomposition potential. They are defined as thermally stable salts synthesized by combining a bulky organic cations with different anions[67]. Unlike the classical electrolytes dissolving salts in molecular solvents, the ionic liquids electrolytes have no solvent molecules. They are generally liquid at room temperature (below 100 °C) and have a high thermal stability, negligible vapor pressure and good electrochemical stability. They can permit an increase in the operating voltage to 3.4V[45] (Figure 2-4), which allows supercapacitors to have higher specific power and energy. However, they are too expensive for commercial applications and also the cyclability of supercapacitors in this novel type of electrolyte is not yet confirmed.

2.6 Fabrications of supercapacitor electrodes

There are a lot of methods for the fabrication of supercapacitor electrodes, including electrodeposition, sol-gel method, chemical precipitation method, electrostatic spray deposition (EDS) and other methods. In this charter, several major methods of electrode fabrications will be presented and discussed.

2.6.1 Electrodeposition

Electrodeposition including electrolytic deposition (ELD) and electrophoretic deposition (EPD) is favored to fabricate the film electrodes due to the low capital investment costs, rigid control of film thickness, uniformity and deposition rate[68]. Although the electrolytically deposited films with very small material loading are far from industrial applications of supercapacitors, electrodeposition methods are still the best way to test the electrochemical capacitance behavior of electrode materials. In contrast, EPD allows much higher deposition rate and higher deposit thickness. This method is promising for the fabrication of bulk electrode materials.

2.6.1.1 The fundamental electrodeposition mechanisms

EPD is achieved via motion of charged particles suspended in a liquid media towards an electrode under an applied electric field. Deposit formation on the electrode is achieved by the coagulation of the particles. ELD is a process in which particles are produced in electrochemical reactions from solutions of metal salts and precipitate at the electrode surface to form deposits. Cathodic or anodic deposits can be obtained depending on the nature of the particle or ion charge. The different mechanisms in EPD and ELD are shown in the figure 2-8.

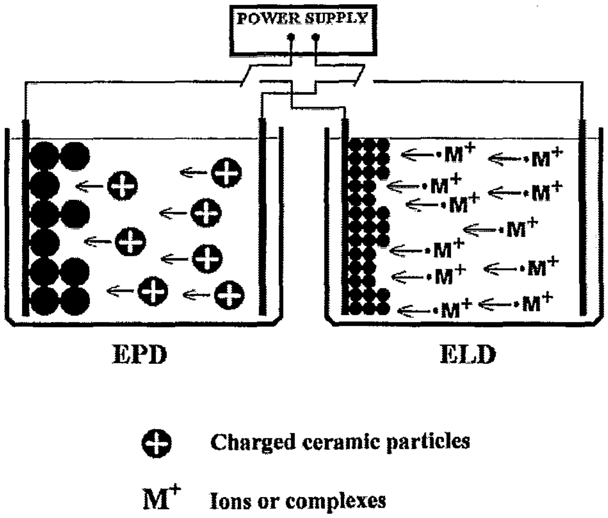

Figure 2-8 Schematic of cathodic electrophoretic deposition and electrolytic deposition, showing electrophoretic motion of positively charged ceramic particles and ions (M^+), followed by hydrolysis of the ions to form colloidal nanoparticles and coagulation of the particles to form EPD and ELD deposits[69].

It is important to note that the deposition rate of the EPD process is much faster than that of ELD, resulting in significantly higher deposit thicknesses[70]. Therefore, EPD is normally utilized to produce thick films while ELD enables the fabrication of the thin nanostructured ceramic films. Figure 2-9 shows the different thickness of coatings can be obtained by EPD and ELD.

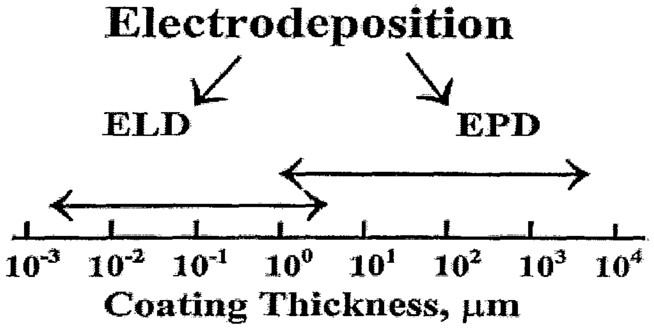

Figure 2-9 Thickness of coatings deposited using ELD and EPD[69].

Solvents function as a vehicle that carries the ceramic particles in suspensions (EPD) or ions in solutions (ELD). The solvents used in electrodeposition must dissolve inorganic salts and organic additives and should be inert with respect to the powder (EPD) and ions (ELD)[69]. Typically, there are two kinds of solvents used for electrodeposition, water and organic liquids. It should be referred that the adsorbed water in deposits can result in shrinkage and cracking during drying while non-aqueous solvents prevent the deposits from hydrating. Hence, in order to obtain a crack-free deposit by ELD, while the sufficient amount of water is required by the formation of particles, mixed solvents in the methanol-water or ethanol-water systems, are favored. The organic liquids are superior to water as a suspension media for EPD. The use of water-based suspensions causes gas formation from the hydrolysis of water, preventing the deposition of a uniform adherent layer and yielding pinholes.

Binders are usually added to suspensions or solutions to increase the adherence and strength of the deposited material and prevent cracking. The optimal amount of binder depends on the particle size and particle surface area[69]. Nonionic-type polymers (polyvinyl alcohol, polyvinyl butyral, ethyl cellulose, and polyacrylamide) are mostly used as binders in EPD, while the cationic polyelectrolytes, such as poly(dimethyldiallylammonium chloride) (PDDA) or polyethylenimine (PEI) with inherent binding properties are favored in ELD and can diminish the cracking problem in electrolytic deposits[71].

In an EPD process, the particles in suspensions must be electrically charged and well dispersed to permit electrophoresis. In aqueous media, the charge at the particle-solvent interface could originate from adsorption or desorption of ions, or dissociation of surface groups. Surfaces of oxide particles dispersed in water tend to coordinate water molecules to form hydroxylated surfaces. The hydroxylated surfaces can be positively or negatively charged depending on pH[69]. Alcohols behave as proton donors for particle charging as well[72], which can ionize to RCH_2O^- and $RCH_2OH_2^+$. Besides, there are a variety of additives can be used to control particle charge in suspensions. Acids, cations (Mg^{2+}, Ca^{2+}, Al^{3+},etc.), organic marcomolecules can be used as charge agents in suspensions[69].

2.6.1.2 Electrodeposition of manganese oxides

Many efforts have been done to electrodeposit manganese oxides in various crystalline and amorphous forms on conductive substrates. The manganese oxide electrodes can be fabricated by EPD and ELD methods. Hu et al.[73] introduced an anodic ELD method by using $MnSO_4 \cdot 5H_2O$ as a manganese precursor. Chang et al.[74] obtained anodic deposits from $Mn(CH_3COO)_2$ by ELD. Chen et al.[75] compared the electrochemical behavior of hydrous manganese oxide from different manganese precursors by anodic ELD, including $Mn(CH_3COO)_2 \cdot 4H_2O$ $MnSO_4 \cdot 5H_2O$, $MnCl_2 \cdot 4H_2O$ and $Mn(NO_3)_2 \cdot 4H_2O$. Meanwhile, Nagarajan et al.[76] obtained cathodic deposits containing nanoparticles of Mn_3O_4 and polyethylenimine (PEI) from PEI-Mn^{2+} solution. Electrochemical oxidation of the films resulted in the formation of electrochemically active MnO_2 phase, which showed high capacitance. Cathodic ELD can also be performed by reduction MnO_4^- species. Manganese oxide films were cathodically deposited on various substrates, such as nickel, stainless steel, and graphite, by reduction of $KMnO_4$[77]. Compared to anodic ELD, cathodic ELD, which can avoid anodic oxidation and dissolution of metallic current collectors, is a much more promising fabrication method for preparing electrodes for supercapacitors. On the other side, manganese oxide particles can be positively charged in the ethanol suspensions, which allow them to be deposited on cathode by EPD[78]. Cheong et al.[79] reported that the well dispersed and stable suspensions of manganese oxide particles can be obtained using sodium alginate as an additive and manganese oxide can be anodic charged and deposited by EPD. Chen et al[80] achieved cathodic EPD of manganese oxide powder using sulfuric acid as additive in ethyl alcohol.

2.6.2 Other methods

Chemical precipitation and sol-gel are wet chemical techniques for material fabrication. The process starts with a chemical solution that reacts to produce colloidal particles of metal oxide. The thin films can be obtained by dip coating or drop coating colloidal materials directly onto substrates. The materials can also be dried and nano-scale powders will form. Then, powders can be mixed with the conductive additives (carbon black, CNT, etc.) and binder to get slurries, then be pasted or penetrated to flat or porous substrates. Lin et al.[81] introduced a sol-gel method to produce manganese oxide electrode for supercapacitor with a SC value of 230 F g^{-1}. The transparent viscous sol was obtained by adding manganese acetate into a citric acid containing *n*-propyl alcohol at room temperature. Xie at al.[54] developed composite materials including MWCNTs and MnO_2 by chemical precipitation methods. Then these powders were mixed with 15% acetylene black and 5% polytetrafluoroethylene to form slurries. The slurries were filled into a foamed nickel and then pressed to form electrodes, which showed a high capacitance value of 250.5 F g^{-1} with a high material loading of about 10 mg. This fabrication method, which allows high material loading of active materials, has a great potential for industrial applications.

Nam et al.[82] reported on the synthesis of porous Mn_3O_4 thin film electrodes by ESD from $MnCl_2 \cdot xH_2O$ precursor solution and suggested that the thin film electrode electrochemically oxidized during the cycling process. The manganese oxide film electrodes also can be deposited from $KMnO_4$ precursor solution, with a SC value of 209 F g^{-1} at low scan rate of 5 mV s^{-1} [83].

Sputter deposition technique have been utilized to fabricate the manganese oxide electrodes for supercapacitors as well[84]. First, the manganese metal was e-beam evaporated and deposited on designed substrates. Then, the manganese layers were oxidized to manganese oxide layer.

2.7 Design of supercapacitors

The specific capacitance value, cell voltage and ESR are three factors which can influence the specific energy and power of capacitors. It will be very critical to enhance capacitance behavior, enlarge the cell voltage and reduce the ESR of supercapacitors.

In order to achieve a high capacitance value, the materials of electrodes are very important, which should have a good electrochemical behavior. Both the electrochemical double-layer capacitance and the pseudocapacitance are interfacial phenomena. Therefore, the materials for supercapacitors should possess a high specific surface area to enhance their charge-storage capability. The high porosity of the electrodes also can improve the capacitance performance of supercapacitors, because the electrolyte ions can be much easier to penetrate into the porous electrodes. It should be mentioned that the porous structure of electrodes has to be tailored for the size and the properties of the electrolytes.

Compared to conventional capacitors, the operating voltage of supercapacitors is generally much lower. The specific energy and power is proportional to the square of operating voltage. The relatively small cell voltage of supercapacitors greatly restricts the specific energy and power. In many practical applications, supercapacitor cells must be series-connected to meet the operating voltage requirements, similar to batteries, which thereby significantly reduce the overall capacitance and increase the total resistance of the cells. In order to overcome the disadvantage of small cell voltage, researchers have implied asymmetric cell design. The asymmetric cell combines Faradaic and non-Faradaic processes by coupling an EDLC electrode with a pseudocapacitor electrode. A hybrid supercapacitor based on activated carbon negative electrode and manganese oxide composite electrode exhibited cell voltage of 2V[85] in aqueous electrolyte. It is also very important to develop new electrolytes allowing a large operating voltage window, such as ionic liquids.

Supercapacitors are known for their high power density. The power characteristics of a cell are proportional to V^2/R where R is the ESR of a cell and V is the operating window. The high ESR can result in reduced specific power. Moreover, it can also result in a low efficiency. Part of the available energy inside supercapacitors is dissipated at the internal resistance ESR. At high power, i.e. high current, this loss can become dominant. There are at least four different contributions to the ESR originating from the (i) electrolyte and separator, (ii) current collector, (iii) contact resistance between the active materials and the current collector and (iv) other contact resistance. In order to achieve a low ESR of supercapacitors, the high conductivity of current collectors and electrolytes is required and the contact resistance between them should be minimal.

Besides the above factors and related aspects, the environment issue, the mechanical and electrochemical stability, and the self-discharge of supercapacitor also should be considered.

Chapter 3 Objective

Supercapacitors are becoming a very popular research topic and manganese dioxide is a promising electrode material. However, there are certain problems related to the fabrication of MnO_2 electrodes. Due to lack of stable Mn^{4+} precursors, the fabrication of high specific area MnO_2 nanoparticles presents difficulties. In the conventional methods, 10-15 wt.% of binders were used for the electrode fabrication. The use of binders resulted in higher resistance and lower capacitance. The porosity, conductivity and utilization of MnO_2 were low, which reduced the electrochemical performance of the electrodes.

The objective of this research is to fabricate advanced electrodes for ES, investigate and optimize the electrochemical performance using industrial current collectors through following engineering aspects:

i) Develop low cost chemical precipitation method suitable for mass production of electrochemically active MnO_2 nanofibers which can largely improve the porosity and surface area of the electrodes for ES.

ii) Develop advanced composite electrodes including MnO_2 and CNTs by impregnation and electrophoretic deposition, which can enhance the conductivity of electrodes

iii) Develop methods for the stabilization of MnO_2 nanoparticles and CNTs in suspensions

Chapter 4 Experiment Procedures

4.1 Starting materials

Reagent grade $KMnO_4$, sodium alginate (Mw = 12 to 80 kDa), sodium dodecyl sulphate, and N-(3-Dimethylaminopropyl)-N-(ethylcarbodiimide hydrochloride) were purchased from Aldrich. Commercial purity multiwall carbon nanotubes were purchased from Arkema. 100 vol.% ethanol was purchased from Commercial Alcohol Inc. Reagent grade polyvinyl butyral binder and phosphate ester were provided by Richard E. Mistler Inc.

4.2 Synthesis of manganese dioxide nanofibers

Manganese dioxide powders for the fabrication of electrodes for ES were prepared by reduction of 0.2M $KMnO_4$ aqueous solutions with ethanol using the reduction reaction:

$$4MnO_4^- + 3CH_3CH_2OH + 4H^+ \rightarrow 4MnO_2 + 3CH_3COOH + 5H_2O \qquad (4\text{-}1)$$

Mixing was performed by slow addition of ethanol to the $KMnO_4$ solution. A dark-brown MnO_2 suspension was obtained. Stirring was performed using a magnetic bar at room temperature during 1-65 h. The powder, obtained by filtration of obtained suspensions, was washed with water to remove potassium ions. Drying was performed in air at 20 °C.

4.3 Electrode fabrication procedures

4.3.1 Impregnation techniques

Impregnation is a widely used electrode fabrication technique, due to its low cost and simple procedure. Impregnation of manganese dioxide and manganese dioxide-carbon nanotube composite powders has been utilized for the fabrication of electrodes for supercapacitors. Aqueous suspensions of manganese dioxide nanofibers and MWCNTs with certain weight ratio were prepared using sodium dodecyl sulphate as a dispersant. The amount of sodium dodecyl sulphate was varied in the range of 0.05-0.1 g L^{-1}. Prior to mixing together, the suspensions of manganese nanofibers and MWCNTs were stirred and then ultrasonically agitated during 30 min. Mixed suspensions were stirred and ultrasonically agitated during 30 min.

Polyvinyl butyral solution in ethanol was prepared and used for the fabrication of MnO_2/MWCNTs slurry, containing 2 wt.% of polyvinyl butyral as a binder . The slurry was used for the impregnation of nickel foams or nickel plaques. Then the impregnated nickel foams or nicke plaques were roller pressed to achieve 20 % of initial thickness. The prepared electrodes were dried in air at room temperature for 24 h.

4.3.2 Anodic EPD of manganese dioxide nanofibers

Anodic EPD was performed from 0-10 g L^{-1} manganese dioxide and 0.1-0.5 g L^{-1} sodium alginate suspensions in a mixed ethanol-water (40 vol.% water) solvent. The volume of the deposition bath was 300 mL. The distance between the substrates and platinum counter electrodes was 15 mm. Constant voltage and constant current power supplies (Amersham Biosciences) were used for electrodeposition. Electrophoretic deposits were obtained at constant voltages of 5-50 V on stainless steel foils, meshes, wires, and graphite substrates. The deposition time was varied in the range of 1-5 min. The deposits were dried at room temperature for 24 hours before weighting. The obained deposits containing alginate were cross-linked in 0.1 M N-(3-Dimethylaminopropyl)-N-(ethylcarbodiimide hydrochloride) solutions for 15 min.

4.3.3 Anodic EPD of manganese dioxide nanofibers and MWCNTs

Anodic EPD was performed from aqueous suspensions containing 0-5 g L^{-1} manganese dioxide, 0.1-0.5 g L^{-1} sodium alginate and 0-0.5 g L^{-1} MWCNTs. Electrophoretic deposits were obtained at constant voltages of 10-50V on stainless steel foils and graphite substrates. The deposits were dried at room temperature for 24 hours before weighting. After deposition, the coatings containing alginate were cross-linked in 0.1 M N-(3-Dimethylaminopropyl)-N-(ethylcarbodiimide hydrochloride) solutions for 15 minutes. The experimental setup for electrodeposition was similar to anodic EPD of manganese dioxide.

4.3.4 Cathodic EPD of manganese dioxide nanofibers

Cathodic EPD was performed from 5-50 g L^{-1} manganese dioxide suspensions in ethanol, containing 0.1-2 g L^{-1} phosphate ester as a dispersant. Electrophoretic deposits were obtained at constant voltages of 10-100 V on stainless steel foils and graphite substrates. The deposition time was varied in the range of 1-5 min. The deposits were dried at room temperature for 24 hours before weighting. The experimental setups for electrodeposition was similar to anodic EPD of manganese dioxide.

4.4 Materials Characterization

X-ray diffraction studies of as-prepared MnO_2 powders were performed with a diffractometer (Nicolet I2) using monochromatic Cu Kα radiation at a scanning speed of 0.5 $°min^{-1}$. Thermogravimetric analysis and differential thermal analysis of the as-prepared powders and deposits were carried out in air at a heating rate of 5 °C min^{-1} using a thermoanalyzer (Netzsch STA-409). Electron microscopy investigations of powders and electrodes were performed using a JEOL 2010F transmission electron microscope and a JEOL JSM-7000F scanning electron microscope equipped with energy dispersive spectroscopy.

4.5 Electrochemical Characterization

Capacitive behavior of the fabricated electrodes was studied using a potentiostat (PARSTAT 2273, Princeton Applied Research) controlled by a computer using a PowerSuite electrochemical software. Electrochemical studies were performed using a standard three-electrode cell containing 0.1-0.5 M Na_2SO_4 aqueous solution, degassed with purified nitrogen gas. The surface area of the working electrodes was 1 cm^2. The counter electrodewas a platinum gauze, and the reference electrode was a standard calomel electrode (SCE). Cyclic voltammetry studies were performed within a potential range of 0-1.0V versus SCE at scan rates of 2-100 mV s^{-1}. The specific capacitance was calculated using half the integrated area of the CV curve to obtain the charge (Q), and subsequently dividing the charge by the mass of the film (m) and the width of the potential window ΔV:

$$C = \frac{Q}{m\Delta V} \tag{4-2}$$

Galvanostatic charge and discharge testing was performed at constant current density in the range of 1-50 mA cm^{-2}. The obtained chronopotentiograms were used for the calculation of SC from the equation:

$$C = \frac{I}{(\Delta E/\Delta t)m} \tag{4-3}$$

where $\Delta E/\Delta t$ is the average slope of the discharge curve in the potential range ΔE, Δt the discharge time and I is the current. The specific power density (S_P) and specific energy density (S_E) were calculated from the chronopotentiograms using the following equations:

$$S_P = \frac{I\,\Delta E}{2m} \tag{4-4}$$

$$S_E = \frac{I\,\Delta E\,\Delta t}{2m} \tag{4-5}$$

Electrochemical impedance spectroscopy has been applied to study the conductivity of the electrodes. . The measurements were performed at open circuit potential with a signal amplitude of 10 mV. The spectra were acquired in a frequency range of 10 mHz-100 kHz. The high frequency value of the real part of complex impedance has been used for the estimation of equivalent series resistance.

Chapter 5 Results and Discussion

5.1 Characterization of MnO_2 nanoparticles

Manganese dioxide nanoparticles were prepared by a chemical precipitation method described in the chapter 4. From the XRD studies and TEM investigations, it is found that manganese dioxide nanofibers have been fabricated and the reaction time can significantly affect the morphology of manganese dioxide powders.

5.1.1 TEM investigations

Figure 5-1 shows the TEM images of as-prepared powers by chemical precipitation at room temperature with reaction time of 1 h. As shown in Figure 5-1a, the large quantity of nanofibers with a length ranged from 0.1 to 1 μm has been observed. The high magnification images (Figure 5-1b and Figure 5-1c) showed that the diameter of nanofibers is about 3-10 nm. The electron diffraction pattern in Figure 5-1d indicates the crystallinity of as-prepared powders.

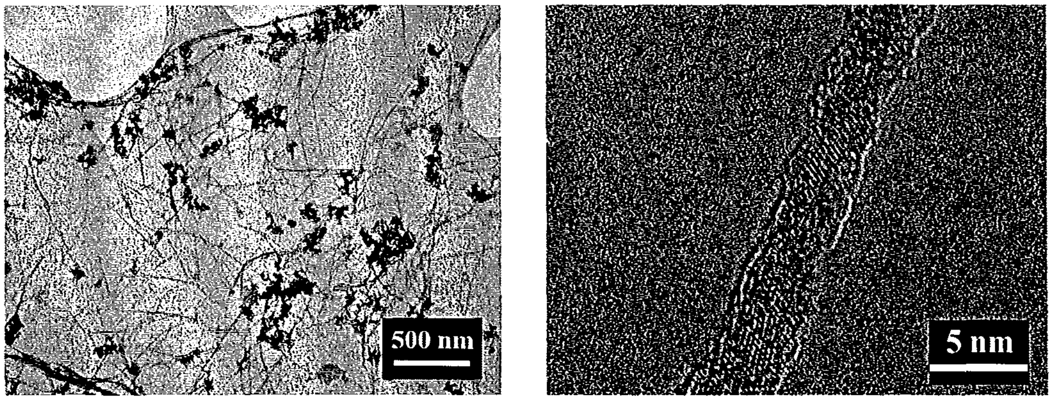

(a) (b)

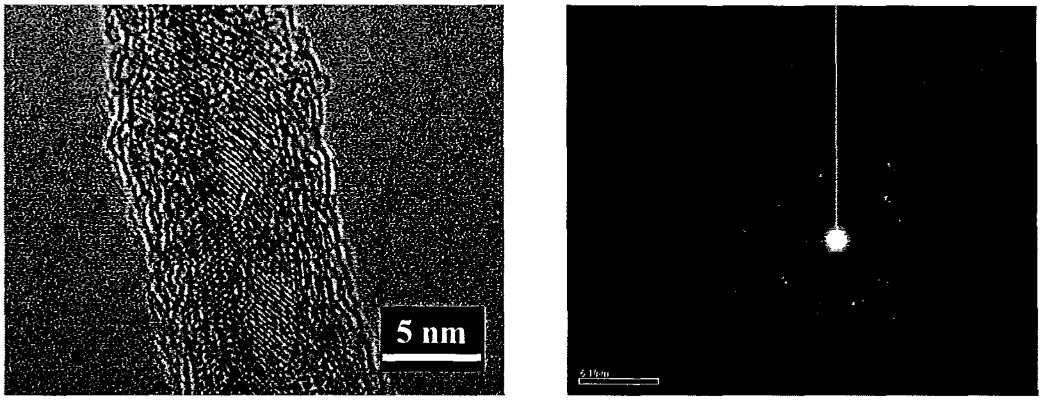

(c) (d)

Figure 5-1 (a) Low magnification TEM image of the MnO_2 powers prepared at room temperature for 1h. (b and c) high magnification TEM images of an individual MnO_2 nanofibers. (d) The SAED pattern of the nanofiber in image c.

Figure 5-2 shows the TEM images of as-prepared powers with reaction time of 20 h. It is shown that some of the individual nanofibers formed bundles (Figure 5-2). It is found that about 2-5 individual nanofibers form a bundle with a diameter about 10-20nm.

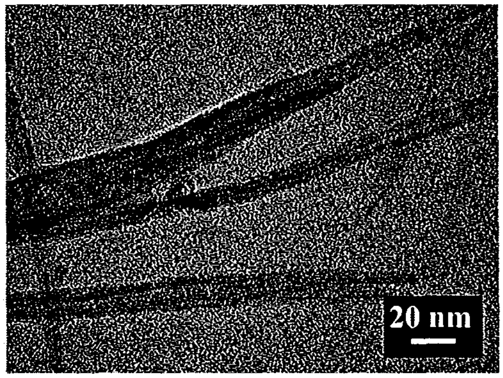

Figure 5-2 TEM image of the MnO_2 powders prepared at room temperature for 20 h.

Figure 5-3 shows the TEM images of as-prepared powders when the reaction time is prolonged to 65 h. It was found that much more nanofibers formed bundles. From the TEM investigation, the bundles obtained at 65 h contain more individual nanofibers than the ones prepared under the reaction time 20 h. Figure 5-3 shows that 10-20 individual nanofibers are involved in a bundle.

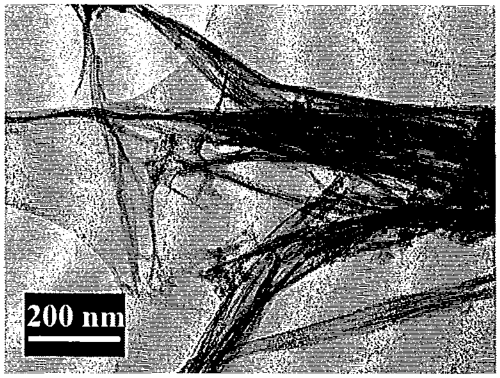

Figure 5-3 TEM image of the MnO_2 powders prepared at room temperature for 65 h.

From the TEM studies of the prepared powders with different reaction time, it is shown that the fibrous nanostructures of manganese dioxide are fabricated. As shown, when the reaction time is 1 h, there are more individual nanofibers. Prolonging the time to 20 h, the MnO_2 bundles started to form. When the reaction time is 65 h, the larger nano-bundles are formed. We speculate that stirring duration is very critical during the formation of the bundles. The stirring provided the possibility for the individual nanofibers to form the bundles and to reduce the surface area. With the stirring time increased, much more fibers are involved in the bundles, as seen from Figure 5-2 and Figure 5-3. The mechanism of the formation of individual nanofibers and bundles should be investigated in the future study.

5.1.2 XRD and EDS studies

XRD studies (Figure 5-4) showed changes in the diffraction patterns of the nanofibers with increasing stirring time. The XRD pattern of the nanofibers stirred during 1 h showed XRD peaks of birnessite, corresponding to the JCPDS file 87-1497. According to the literature, birnessite has a two-dimensional layered structure that consists of edge shared MnO_6 octahedra with cation and water molecules occupying the interlayer regions[86]. The birnessite formula is generally expressed as $A_xMnO_{2+y}(H_2O)_z$, in which A represents an alkali metal cation. The average oxidation state of Mn usually falls between 3.6 and 3.8, which represents a predominance of Mn^{4+} with minor amounts of Mn^{3+} and Mn^{2+} [86]. The intensity of the peaks of the birnessite phase decreased with increased stirring time, indicating lower crystallinity. After 20 h of stirring the XRD pattern showed very small broad peaks. It was suggested that the nanofibers contained crystalline and amorphous phases. It was found that precipitated powders contained K and adsorbed water. EDS studies showed the K/Mn ratio of 0.16±0.03 and 0.14±0.03 for powders stirred during 1 and 20 h, respectively.

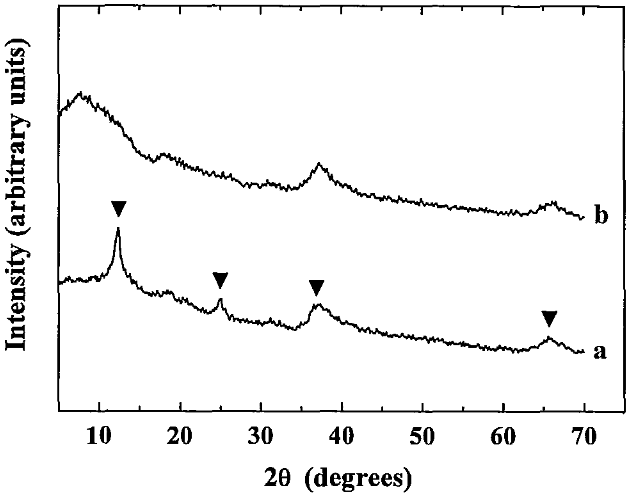

Figure 5-4 X-ray diffraction patterns for powders, containing nanofibers stirred during (a) 1 h and (b) 20 h (▼ - JCPDS file 87-1497).

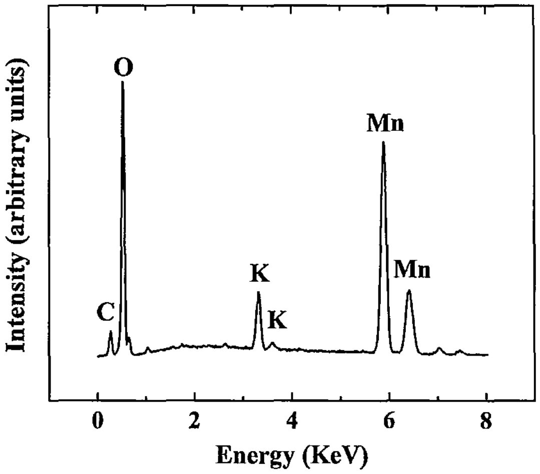

Figure 5-5 EDS data for as-prepared MnO_2 powders with reaction time 20 h.

5.1.3 TGA&DTA studies

Figure 5-6 shows TGA and DTA data for manganese dioxide nanofibers with reaction time of 20 h. TGA data showed a sharp reduction in sample weight below 200 °C, then sample weight decreased gradually with increasing temperature. Observed weight loss of 17.7 wt.% at 430 °C can be related to dehydration of the prepared powders. Weight gain of 0.7 wt.% observed in the range of 430-475 °C can be attributed to oxidation. The reduction in sample weight was observed in the range of 630-850 °C. Additional steps in weigh loss were recorded at 850-890 and 940-965 °C. The decrease in sample weight at temperatures exceeding 630 °C can be attributed to reduction of manganese dioxide and formation of Mn_3O_4 phase at elevated temperatures[87]. The total weight loss at 1200 °C was found to be 23.3 wt%. The DTA data (Figure 5-6) showed a broad endotherm around 100 °C, which can be attributed to deposit dehydration. The exotherm at 455 °C can be attributed to oxidation in agreement with corresponding TGA data. The endotherms at 880 and 950 °C are related to corresponding steps in weight loss and can be attributed to reduction of manganese dioxide.

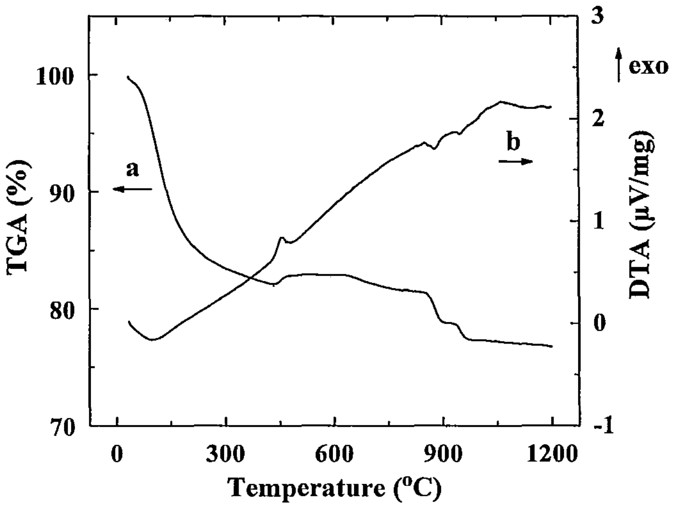

Figure 5-6 (a) TGA and (b) DTA data for as-prepared MnO_2 with reaction time 20 h.

5.2 Nickel foam based composite electrodes

Porous nickel foams are in high demand for applications in batteries[88, 89] and ES[90]. In the batteries and supercapacitors, nickel foams are used as high surface area current collectors, containing highly accessible active material within their conducting light weight web, which provides structural strength. The high porosity and large pore size of nickel foams allow for easy impregnation of the active material slurry into the porous current collectors. However, the increase in foam porosity resulted in reduced conductivity[88]. This problem has been addressed by the use of conductive additives, which formed a secondary conductivity network within the nickel foam cells[88].

Similar approach can be used for the fabrication of ES. In this work, composite electrodes containing MnO_2 nanofibers and MWCNTs were prepared by impregnation of porous nickel foam. The total mass in the composite electrodes was 40 mg cm^{-2}. The impregnated INCOFOAM® (Figure 5-7a) was roller pressed to ~20% of initial thickness in order to achieve final porosity of 30%[88]. The use of nickel foam current collectors together with CNTs, which provided a secondary conductivity network, enabled good conductivity, better utilization of the active material and improved porosity. It was suggested that composite materials containing MnO_2 nanofibers and MWCNTs had an advantage of improved contact between two different fibrous materials compared to composites of spherical particles of the same mass. MnO_2 nanofibers and MWCNTs can form a porous fibrous network, which is beneficial for the electrolyte access to the active material. The use of MWCNTs as conductive additives has benefits of high surface area and low percolation threshold. According to the manufacturer, the average diameter of the MWCNTs used in this study was ~15 nm and length ~0.5 µm (Figure 5-7b).

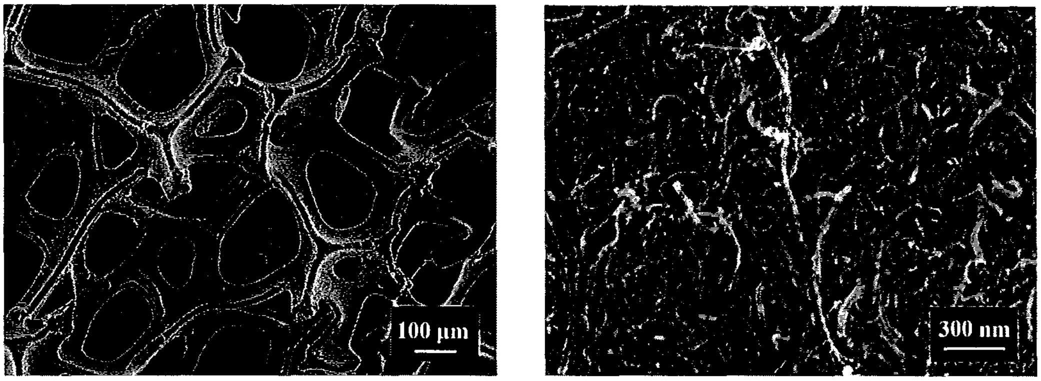

(a) (b)

Figure 5-7 SEM image (a) INCOFOAM® and (b) MWCNTs.

Figure 5-8 shows SEM images of impregnated and roller pressed electrodes. The SEM images at different magnifications of the electrode surface showed porosity (Figure 5-8a and Figure 5-8b). The SEM image of the fracture of the electrode (Figure 5-8c) indicated that active material filled the voids in the nickel foam.

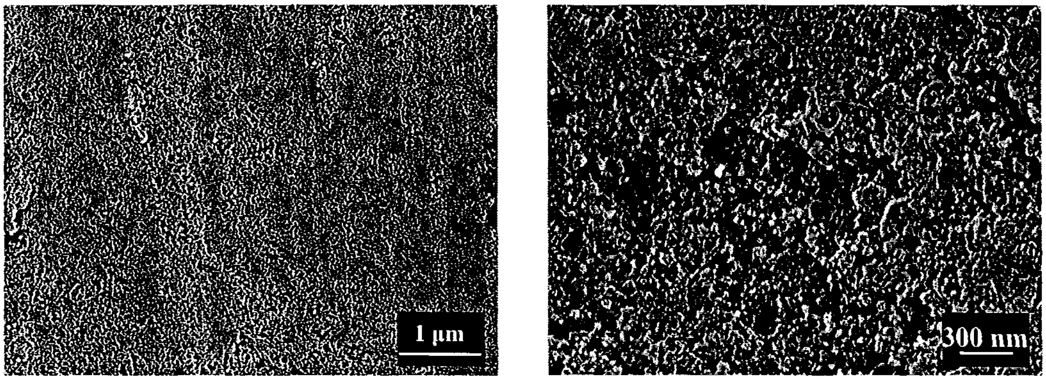

(a) (b)

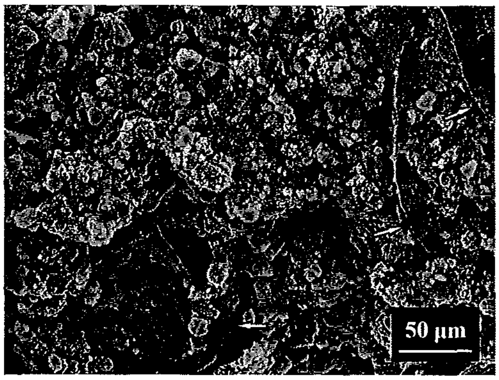

(c)

Figure 5-8 SEM images of a composite electrode, containing 15 wt.% of MWCNTs. (a and b) Surface at different magnifications and (c) fracture. Arrows show Ni foam.

In this investigation, the highest SC of the composite electrodes was 155 F g^{-1} at a scan rate of 2 mV s^{-1} in the 0.5 M Na_2SO_4 solutions. It is more than 2 times higher compared to the literature data for electrodes of similar mass[85]. This is the result of the use of advanced current collector, advanced particle fabrication method and advanced microstructure. The influence of active material composition and electrolyte concentration on the capacitive behavior of the composite electrodes was studied.

5.2.1 Effect of electrolyte concentration and scan rate

Electrochemical testing in the 0.1-0.5 M Na_2SO_4 solutions revealed capacitive behavior of the composite electrodes. Figure 5-9 shows typical CVs at different scan rates. The box shape of the CVs and the increase in current with increasing scan rate indicated good capacitive behavior in the 0.5M Na_2SO_4 solutions (Figure 5-9 a-d). However, the comparison of the CVs obtained at the scan rate of 20 mV s^{-1} in the 0.5 and 0.1 M Na_2SO_4 solutions (Figure 5-9d and Figure 5-9e) showed a smaller area of the CV obtained in the 0.1 M Na_2SO_4 solutions, which was related to lower SC. Moreover, the CV shape in the 0.1 M Na_2SO_4 solutions deviated significantly from the ideal box shape. The difference can be attributed to the lower conductivity of the 0.1 M Na_2SO_4 solutions and diffusion limitations in pores of the composite electrodes. The CV testing result of the composite electrodes was in a good agreement with the experimental data shown in Figure 5-10. Higher SC was obtained in the 0.5 M Na_2SO_4 solutions compared to the 0.1 M Na_2SO_4 solutions for the samples of the same mass and composition. Therefore, further testing was performed in the 0.5 M Na_2SO_4 solutions. The highest SC of 155 F g^{-1} was obtained at a scan rate of 2mVs^{-1} in the 0.5 M Na_2SO_4 solutions. The SC decreased with increasing scan rate for electrodes of fixed composition as shown in Figure 5-10. The decrease in SC with increasing scan rate can be attributed to the diffusion limitations in pores.

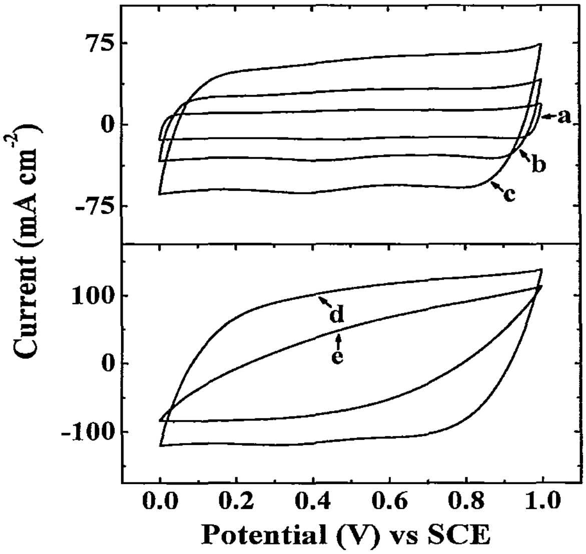

Figure 5-9 CVs for the composite electrode, containing 15 wt.% MWCNTs, tested at scan rates of (a) 2 mV s^{-1}, (b) 5 mV s^{-1}, (c) 10 mV s^{-1}, (d and e) 20 mV s^{-1} in (a-d) 0.5 M and (e) 0.1 M Na_2SO_4 solutions.

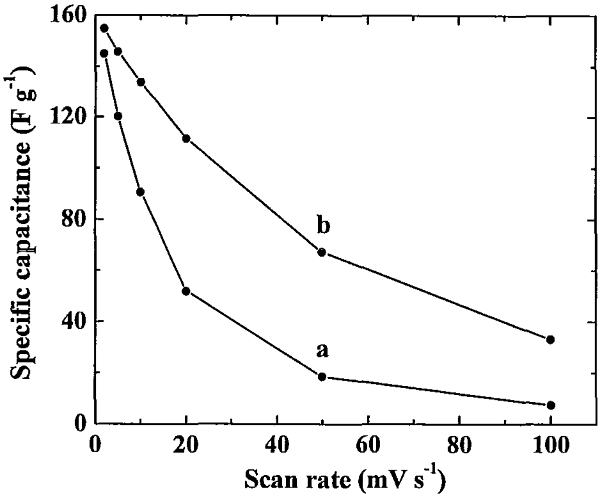

Figure 5-10 Specific capacitance for composite electrodes, containing 15 wt.% MWCNTs tested in (a) 0.1 M Na_2SO_4 and (b) 0.5 M Na_2SO_4 solutions.

5.2.2 Effect of active material composition

Figure 5-11 shows the influence of active material composition on the capacitive behavior of the electrodes. For manganese dioxide electrodes, the relatively small area of the CV indicated poor capacitive behavior. The SC at a scan rate of 2 mV s^{-1} was only 22 F g^{-1} and decreased rapidly with increasing scan rate (Figure 5-12). It can be attributed to the insulating properties of the manganese dioxide. This result also indicated that the conductivity of the Ni foam was insufficient. The additional conducting network, provided by MWCNTs, improved the capacitive behavior of the composite electrodes. The composite electrodes containing MWCNTs showed box shape CVs (Figure 5-11). The electrodes, containing 10 and 20 wt.% MWCNTs, showed SC of 145 and 150 F g^{-1}, respectively, at a scan rate of 2 mV s^{-1}. It is important to note that the improvement in capacitive behavior with increasing

MWCNTs concentration was especially evident at higher scan rates (Figure 5-12). The increase in MWCNTs content from 10 to 20 wt.% resulted in increase in SC from 61 to 118 F g^{-1} at a scan rate of 20 mV s^{-1}, and from 32 to 79 F g^{-1} at a scan rate of 50 mV s^{-1}. The increase in SC can be attributed to increasing conductivity of the composite materials and changes in the composite microstructure associated with increasing MWCNTs content from 10 to 20 wt.%. Recent studies showed that MWCNTs can reduce the aggregation of nanoparticles of active material, inducing better distribution of the particles in the netlike MWCNTs structure[91]. Reduced agglomeration of the particles resulted in improved electrochemical performance of the composite electrodes.

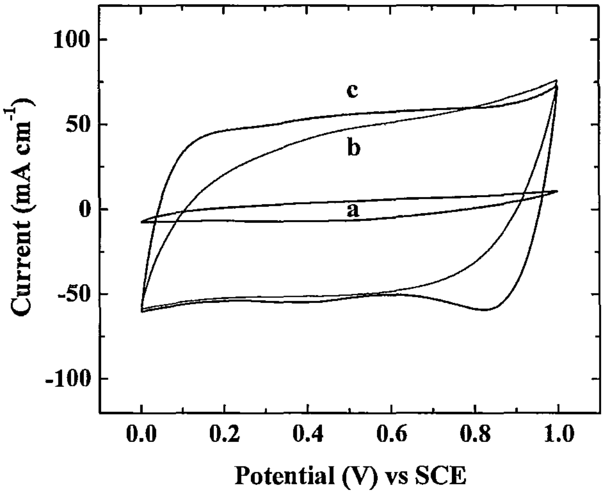

Figure 5-11 CVs at a scan rate of 10 mV s^{-1} for composite electrodes containing (a) 0 wt.%, (b) 10 wt.% and (c) 20 wt.% MWCNTs tested in the 0.5 M Na_2SO_4 solutions.

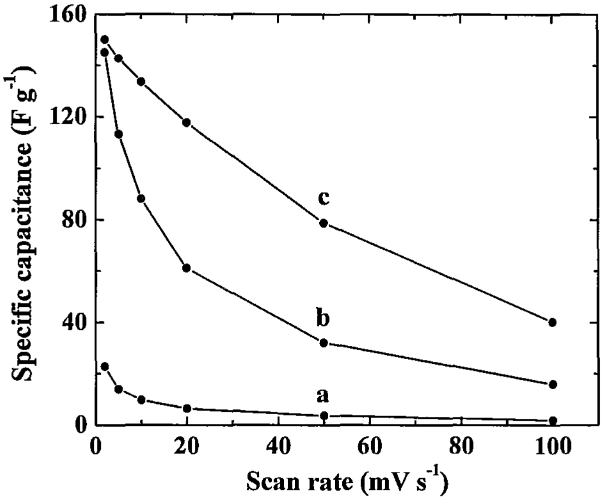

Figure 5-12 Specific capacitance vs. scan rate for composite electrodes containing (a) 0 wt.%, (b) 10 wt.% and (c) 20 wt.% MWCNTs tested in the 0.5 M Na_2SO_4 solutions.

The increase in scan rate has a direct impact on the diffusion of ions, since at high scan rates ions approach only the outer surface of the electrode material[92] The MWCNTs content in the composite electrodes is an important factor controlling electronic conductivity of the materials. The investigation of NiO-MWCNTs composites[93] showed the enhancement in the conductivity and SC for MWCNTs content higher than the percolation limit of 10 wt.%. The investigation of manganese dioxide/MWCNTs composites[94] showed that the 10-15 wt.% MWCNTs additive increased the SC from 0.1 to 140 F g^{-1}. It was found that MWCNTs generated an open porous network, which facilitated the electrolyte access to the active material. Moreover, extended polarization window was achieved in the manganese dioxide/MWCNTs composites[94]. The study[94] highlighted the advantages of MWCNTs compared to other conductive additives and showed improved capacitive behavior at a scan rate of 2 mV s^{-1}. Our testing results indicate that significant improvement in capacitive behavior can be achieved at higher scan rates when MWCNTs are used as conductive additive for the fibrous manganese dioxide active material and using INCOFOAM® current collectors. The microstructure and composition of the composite electrodes can be further optimized by the variation of materials loading, electrode thickness, porosity and MWCNTs content in the composites.

5.2.3 Impedance spectroscopy and chronopotentiometry studies

Figure 5-13 shows charge-discharge behavior of the composite electrode at a current density of 50 mA cm^{-2}. The discharge curve is nearly linear, however initial voltage drop was observed, which can be attributed to electrode resistance. According to Equation 4-4 and Equation 4-5, for the composite electrode with materials loading of 40 mg cm^{-2}, a power density of 0.625 kW kg^{-1} was obtained at an energy density of 17.36 Wh kg^{-1}. Figure 5-14 shows complex impedance of the electrode in the frequency range of 100 mHz to 70 kHz. The equivalent circuit for ES was discussed in detail by Conway[1]. The high frequency value of the real part of complex impedance has been used for the estimation of equivalent series resistance which was found to be ~ 0.5 Ohm. It is suggested that the further optimization of electrode composition and microstructure will result in reduced resistance and improved capacitive behavior.

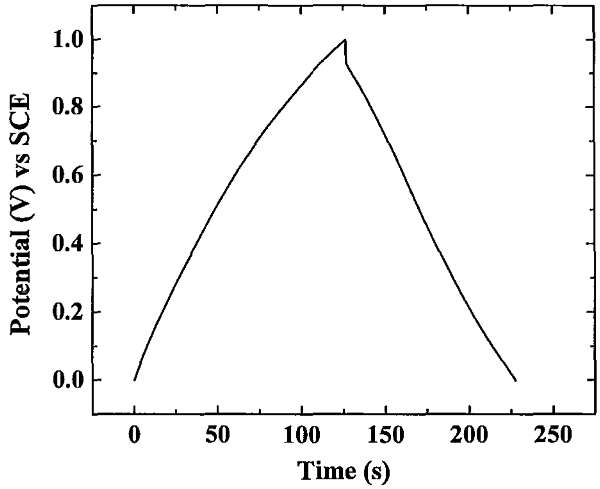

Figure 5-13 Chronopotentiometry data for a composite electrode containing 20 wt.% MWCNTs at a current density 50 mA cm^{-2} in the 0.5 M Na_2SO_4 solution.

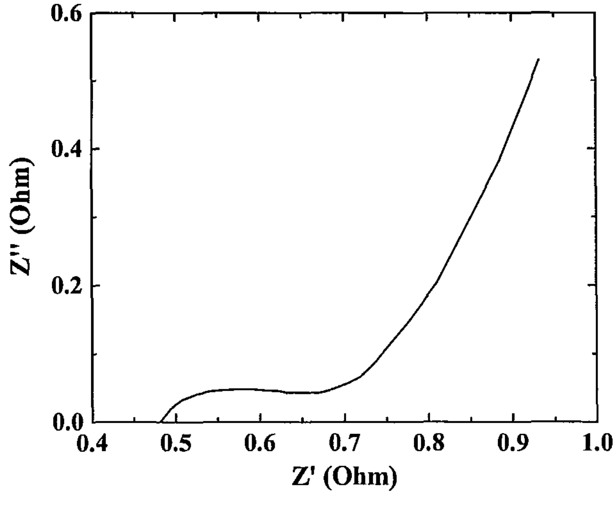

Figure 5-14 Nyquist plot for complex impedance $Z^* = Z' - iZ''$ of the composite electrode containing 20 wt.% MWCNTs in the 0.5 M Na_2SO_4 solution.

5.3 Nickel plaque based composite electrodes

In addition to nickel foam, nickel plaque is another type of nickel material, which is also widely used in industry for the fabrication of electrodes for rechargeable batteries[95]. Active materials are impregnated chemically or electrochemically into the porous nickel structures, which are used as current collectors[96]. Nickel plaques are current collectors of choice for battery applications demanding high power and reliability, along with long cycle life, such as batteries for aerospace and railway applications, power tools, and some portable electronics[95]. The pore size of nickel plaques is smaller compared to that of foams. The smaller pore size decreases the distance for electrons to travel from the current collector into the active material during cell discharge, and consequently improves the discharge rate characteristics for high power applications[96].

The goal of this work was the fabrication and investigation of composite electrodes containing MnO_2 nanofibers and MWCNTs by impregnation of porous nickel plaques. In the composite electrodes, MWCNTs formed a secondary conductivity network within the porous nickel structure. Obtained composite electrodes, containing 15 wt.% MWCNTs with total mass loading of 7-14 mg cm^{-2}.

Nickel plaques were provided by Inco Company. Figure 5-15a shows a schematic of the cross section of a nickel plaque, which consist of a perforated nickel foil and sintered nickel particles. The voids between the particles provide a space for the loading of the plaques with active materials. Figure 5-15b and Figure 5-15c show

SEM images of the surface of a nickel plaque at different magnifications. The plaques exhibit porous microstructure with pore size in the range of 1-50 μm (Figure 5-15b). The SEM image obtained at higher magnification (Figure 5-15c) shows small particle size of nickel particles in the range of 0.5-3 μm, which forms a conductive porous matrix. It was suggested that high surface area, small particle size, porosity and conductivity of nickel plaques are beneficial for application in ES. The SEM image of the impregnated material shows porous fibrous microstructure (Figure 5-16).

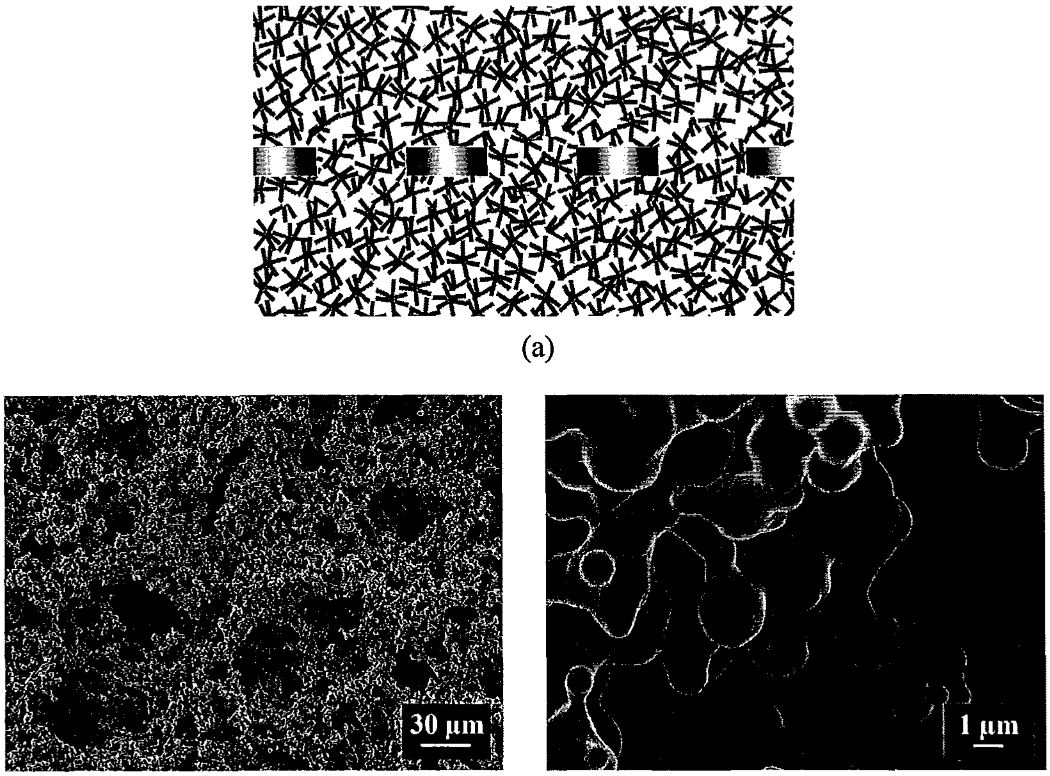

(a)

(b) (c)

Figure 5-15 (a) Schematic of a cross section of a Ni plaque, containing perforated Ni foil and sintered Ni particles and (b, c) SEM images of the surface of a nickel plaque at different magnifications.

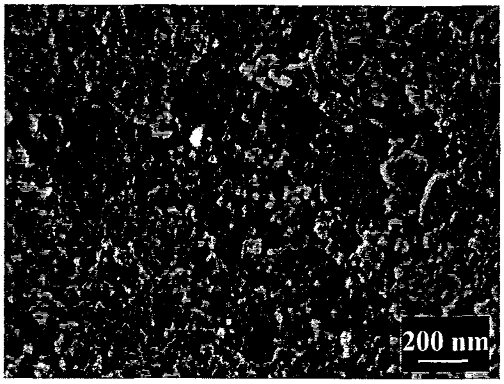

Figure 5-16 SEM image of a composite electrode containing MnO_2 nanofibers and MWCNTs

In this approach, porous nickel current collectors provided the improved contact with active materials and better conductivity at relatively high materials loading. The obtained composite electrodes showed a capacitive behavior in the 0.5 M Na_2SO_4 solutions.

5.3.1 Capacitive behavior studies of composite electrodes

Figure 5-17 shows typical CVs for the composite electrode with material loading of 7 mg cm^{-2}. Within the potential range of 0-1.0 V versus SCE the composite electrode exhibited capacitive-like current-potential responses, indicated by the box shape of the CVs. It is clear from Figure 5-17 that there are no redox peaks in the range between 0 and 1.0 V. Figure 5-18 shows SC at different scan rates for the composite electrodes. The SC decreased with increasing scan rate due to the diffusion limitations in pores. However, decreasing rate was much slower than that of the nickel foam based composite electrodes. It should be related to the use of nickel plaque current collectors. The high SC at high scan rates is important for the fabrication of ES with high power characteristics. The electrodes prepared using powders stirred during 1 h showed higher SC compared to the powders stirred during 20 h. This can be attributed to low agglomeration of the powders stirred during 1 h. This result indicated that further optimization of the powder processing conditions can be beneficial for the improvement of the electrode performance. The highest SC of 185 F g^{-1} was achieved at a scan rate of 2 mV s^{-1} for material loading of 7 mg cm^{-2}. However, the SC decreased significantly with increasing material loading (Figure 5-19). The reduction in the SC is especially evident at a scan rate of 100 mV s^{-1}.

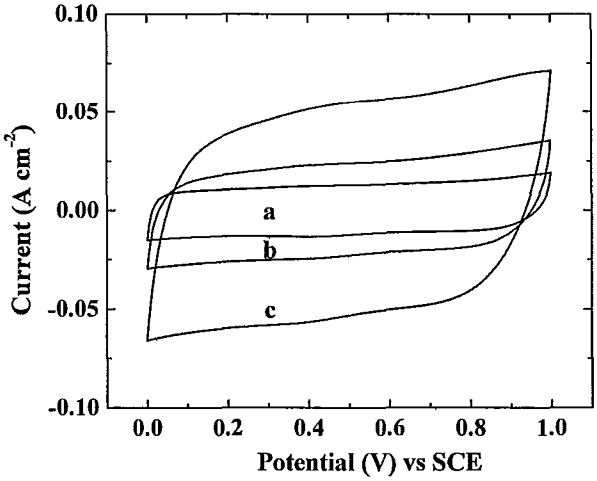

Figure 5-17 CVs for a composite electrode containing MnO_2 nanofibers stirred during 1 h, mixed with MWCNTs and impregnated into a nickel plaque with material loading of 7 mg cm^{-2} at scan rates of (a) 10, (b) 20 and (c) 50 mV s^{-1}.

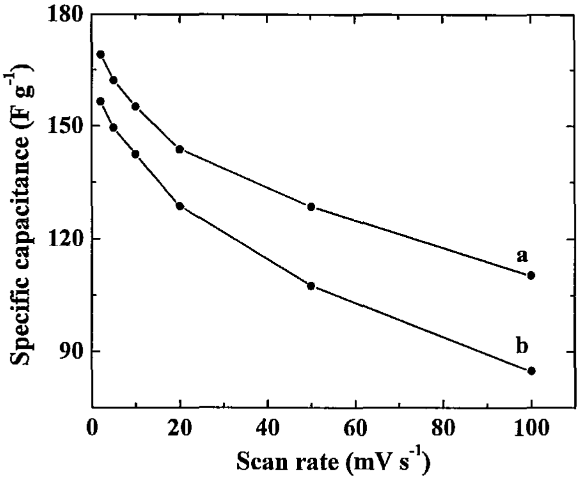

Figure 5-18 Specific capacitance versus scan rate for composite electrodes containing MnO_2 nanofibers stirred during (a) 1 h and (b) 20 h, mixed with MWCNTs and impregnated into nickel plaques with material loading of 10 mg cm^{-2}.

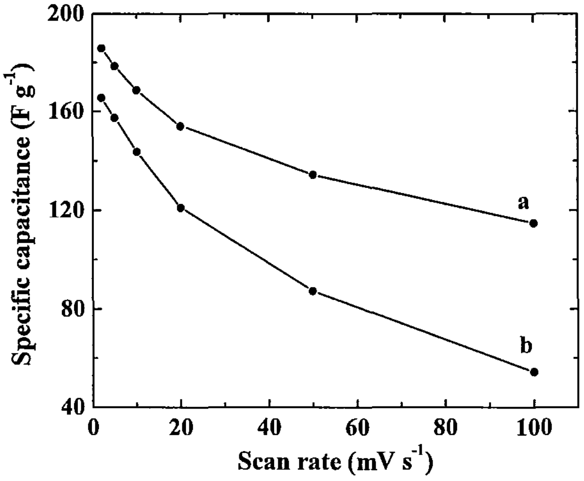

Figure 5-19 Specific capacitance versus scan rate for composite electrodes containing MnO_2 nanofibers stirred during 1 h, mixed with MWCNTs and impregnated into nickel plaques with material loading of (a) 7 mg cm^{-2} and (b) 14 mg cm^{-2}.

5.3.2 Impedance spectroscopy and chronopotentiometry studies

Figure 5-20 shows charge-discharge behavior for the composite electrode with material loading of 10 mg cm^{-2}. The charge-discharge curves obtained at different current densities were nearly linear and indicated good capacitive behavior in agreement with box shape CVs shown in Figure 5-17. According to Equation 4-4 and Equation 4-5, for the composite electrode with material loading of 10 mg cm^{-2}, a maximum energy density of 22.22 Wh kg^{-1} was obtained at an power density of 1 kW kg^{-1}. Figure 5-21 shows impedance spectroscopy data for the sample with the same mass. The equivalent circuit of ES was discussed in the literature and included RC transmission line, describing the porous electrode[97]. C_n elements represent double layer capacitance and pseudo capacitance, whereas R_n elements represent electrolyte resistance in pores, Faradaic resistance and equivalent series resistance of the electrodes[20]. Conway and Pell described the impedance of porous electrode using 5 element (n=5) circuit[97]. A CPE impedance element, rather than a pure capacitance C, was used in another investigation[98]. The CPE element describes a 'leaking' capacitor with microscopic roughness of the surface and capacitance dispersion of interfacial origin. The equivalent circuits should allow an optimum representation of the measured spectra with a minimum set of model parameters. Good agreement of simulated and measured data (Figure 5-21) was found for the equivalent circuit similar to that proposed for composite ruthenium oxide-graphite electrodes[99]. In this circuit C_1 and R_1 described double layer capacitance and charge transfer resistance, respectively. Q_2 described impedance of porous electrode and R_2 represented electrolyte resistance. The high frequency Z' value of the complex impedance

Z=Z'-*i*Z" showed that $R=R_1+R_2$ is about 0.4 Ohm for the electrode with area of 1 cm^2. Relatively low resistance R is beneficial for high power ES[20].

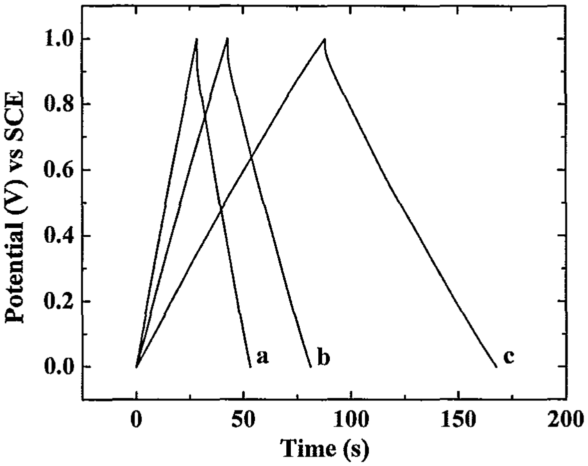

Figure 5-20 Chronopotentiometry data for a composite electrode containing MnO_2 nanofibers stirred during 1 h, mixed with MWCNTs and impregnated into nickel plaques with material loading of 10 mg cm^{-2} at current densities of (a) 60 (b) 40 and (c) 20 mA cm^{-2}.

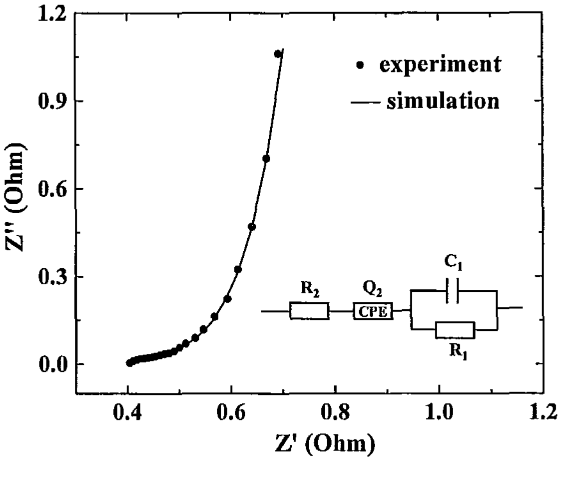

Figure 5-21 Impedance data for composite electrode containing MnO_2 nanofibers stirred during 1 h, mixed with MWCNTs and impregnated into nickel plaques with material loading of 10 mg cm^{-2}.

5.4 Anodic EPD of MnO_2 nanofibers

In order to avoid the microstructure damage by pressing in the impregnation techniques, EPD was employed to fabricate the film electrodes, which can also be used to further study the electrochemical capacitive behavior of as-prepared MnO_2 nanofibers. The experiment procedure was discussed in the chapter 4.

In this approach, the problem related to the stabilization of the high concentration of MnO_2 suspension was solved. Obtained results indicate that EPD is a promising method for the fabrication of manganese dioxide electrodes for ES. The highest SC of 412 F g^{-1} was observed for the 50 μm cm^{-2} film electrode at a scan rate of 2 mV s^{-1}.

5.4.1 Deposition yield

Manganese dioxide nanofibers were used for the fabrication of films by EPD. However, the suspensions of manganese dioxide nanofibers were unstable and exhibited rapid sedimentation when the ultrasonic treatment was interrupted. It was found that the addition of sodium alginate to the manganese dioxide suspensions enabled the formation of well-dispersed suspensions, which were stable against sedimentation for 1-2 days. Sodium alginate was an effective dispersant and binder for the anodic EPD of MnO_2 nanofibers. Sodium alginate[100] is a weak anionic polyelectrolyte, which is negatively charged in aqueous solutions at pH> 3. In the suspension, sodium alginate dissociates to sodium ions and alginate ions, then the MnO_2 nanofibers will absorb the alginate ions when PH>3, hence MnO_2 is negatively charged. This approach enabled electrostatic stabilization of charged MnO_2 particles in suspensions. When an electrical field was applied, the negatively charged MnO_2 particles moved to the anode. At the anode surface due to the decomposition of water, the pH near the anode decreases to smaller than 3. The absorbed alginate ions reacted with H^+, neutralized and the MnO_2 was deposited on the anode.

EPD experiments showed the formation of anodic deposits on stainless steel substrate. The increase in deposition time resulted in an increasing deposit mass, indicating the formation of deposits of various thickness (Figure 5-22). The increase in deposition voltage resulted in higher deposition yield (Figure 5-22). These results are in a good agreement with Hamaker equation[101], which predicts an increase in the deposit mass M with increasing deposition time t:

$$M = \mu EtSC \qquad (5\text{-}1)$$

where μ is particle mobility in an electric field $E = U/d$, $U = U_{app} - U_{dep}$, U_{app} is applied voltage , U_{dep} is voltage drop in the deposit, d is distance between electrodes, C is suspension concentration, S is electrode area. However, the Hamaker equation cannot explain non-linear increase in deposit mass with increase in the deposition voltage observed in this investigation (Figure 5-23).We suggest that the electrophoresis of manganese dioxide nanofibers, which have a high aspect ratio, can be described by the equations derived for infinitely long cylindrical colloidal particles[102]:

$$\mu_{\perp} = \varepsilon_r \varepsilon_0 \zeta / 2\eta \qquad (5\text{-}2)$$

$$\mu_{\parallel} = \varepsilon_r \varepsilon_0 \zeta / \eta \qquad (5\text{-}3)$$

where $\mu_\perp$ and $\mu_\parallel$ are electrophoretic mobilities in transverse and tangential directions, respectively, ε_r is the relative permittivity of the medium, ε_0 is the permittivity of vacuum, ζ is zeta potential and η is viscosity. It is suggested that the increase in electric field can result in increasing orientation of the manganese dioxide nanofibers parallel to the direction of an electric field. Equation 5-2 and 5-3 indicate that $\mu_\parallel > \mu_\perp$. Therefore, such orientation can result in higher electrophoretic mobility and higher deposition rate. It is in this regard that recent studies showed electric field dependent orientation of carbon nanotubes parallel to electric field[103]. The orientation was attributed to high dipole moment of the nanotubes, which resulted from the shape anisotropy. However, it is important to note that electrophoresis results in accumulation of charged particles at the electrode surface and not necessarily results in the deposit formation. Recent studies showed that electrostatic repulsion of charged particles at the electrode surface can prevent deposit formation[69]. On the other hand, particle coagulation and deposit formation can be enhanced in stronger electric fields[69]. Therefore, non-liner increase in deposit mass with increase in the deposition voltage can be also attributed to the influence of electric field on deposit formation.

Turning again to the experimental data shown in Figure 5-22 and 5-23, it is seen that the concentration of particles in suspensions for EPD and deposit yield are comparable with the corresponding literature data for electrophoretic deposition of other materials[69]. Therefore, the results of this work indicated that difficulties related to the formation of stable MnO_2 suspensions[104] of desired concentration can be avoided and EPD can be used for the deposition of MnO_2 films at a practically important deposition rate.

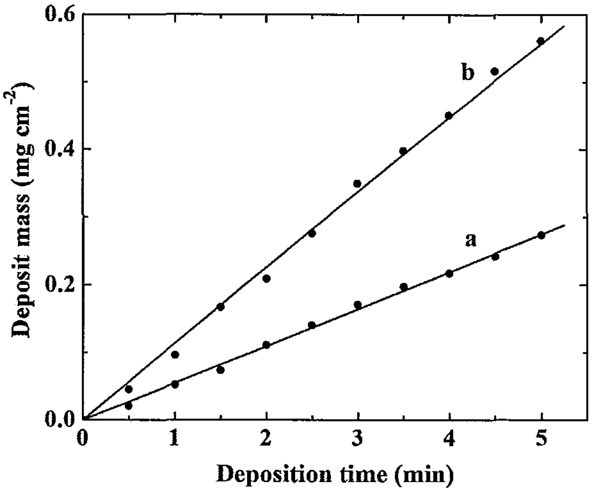

Figure 5-22 Deposit mass versus deposition time for the deposits obtained from 3 g L^{-1} manganese dioxide suspensions on stainless steel substrates at deposition voltages of (a) 15 V and (b) 25 V.

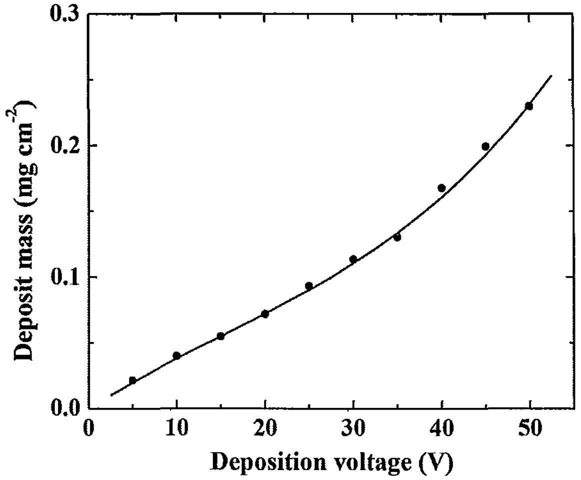

Figure 5-23 Deposit mass versus deposition voltage for the deposits obtained from 3 g L^{-1} MnO_2 suspensions on stainless steel substrates at deposition time of 1 min.

5.4.2 SEM investigations of deposits

Figure 5-24 shows SEM images of MnO_2 films prepared by EPD on a stainless steel foil (a and b) and mesh (c and d). Low magnification image (Figure 5-24a) indicates that obtained films are crack free. EPD resulted in relatively uniform deposition on substrates of complex shape such as stainless steel mesh (Fig 5-24c). The SEM images at higher magnifications showed fibrous microstructure of the films (Figure 5-24b and 5-24d). The deposits consisted of individual nanofibers and bundles. This SEM observation is in a good agreement with the TEM data for as-prepared powders (Figure 5-1). The SEM images showed film porosity with a pore size of about 10-50 nm. The results of SEM investigations indicated that films of different thickness in the range of 2-100 μm can be obtained by variation of the deposition time and voltage. As an example, Figure 5-25a and Figure 5-25b show SEM images at different magnifications of fracture of a film deposited on a graphite substrate. The thickness of the film is about 4 μm. SEM images indicated porosity of the deposited film. An SEM image (Figure 5-25c) of the film on a graphite rod indicated relatively uniform deposition. The thickness of the film shown in Figure 5-25d is about 70 μm.

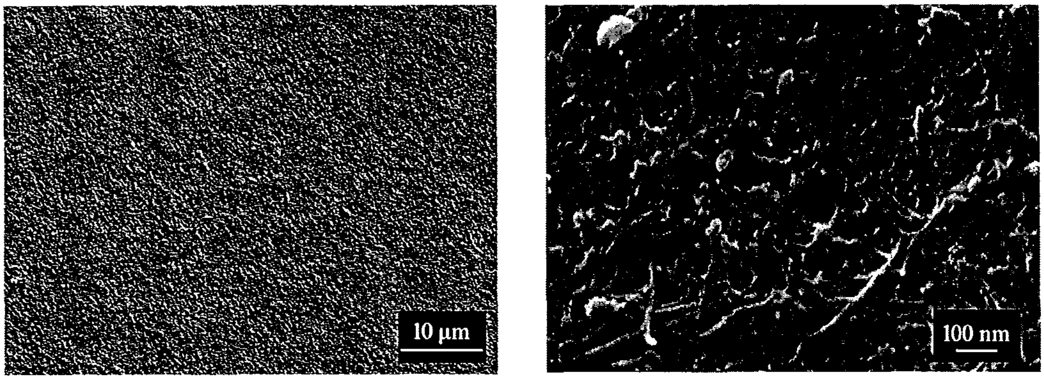

(a) (b)

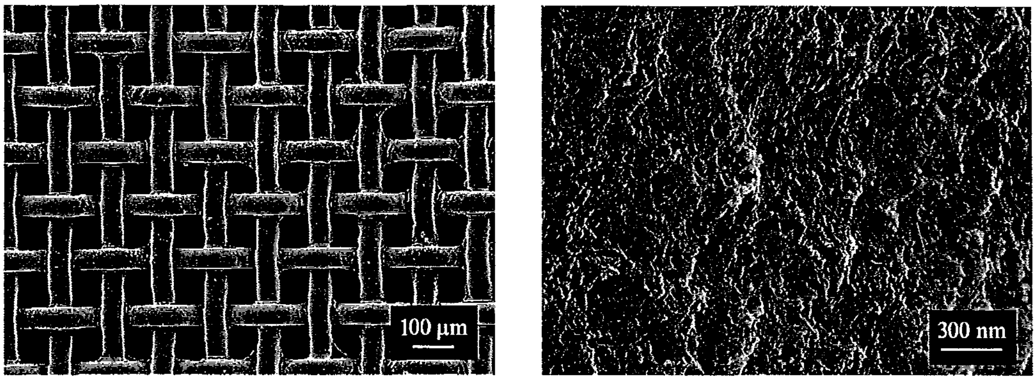

(c) (d)

Figure 5-24 SEM images at different magnifications for deposits obtained from 3 g L^{-1} MnO_2 suspensions on (a and b) stainless steel foil and (c and d) stainless steel mesh at deposition voltage of 15 V.

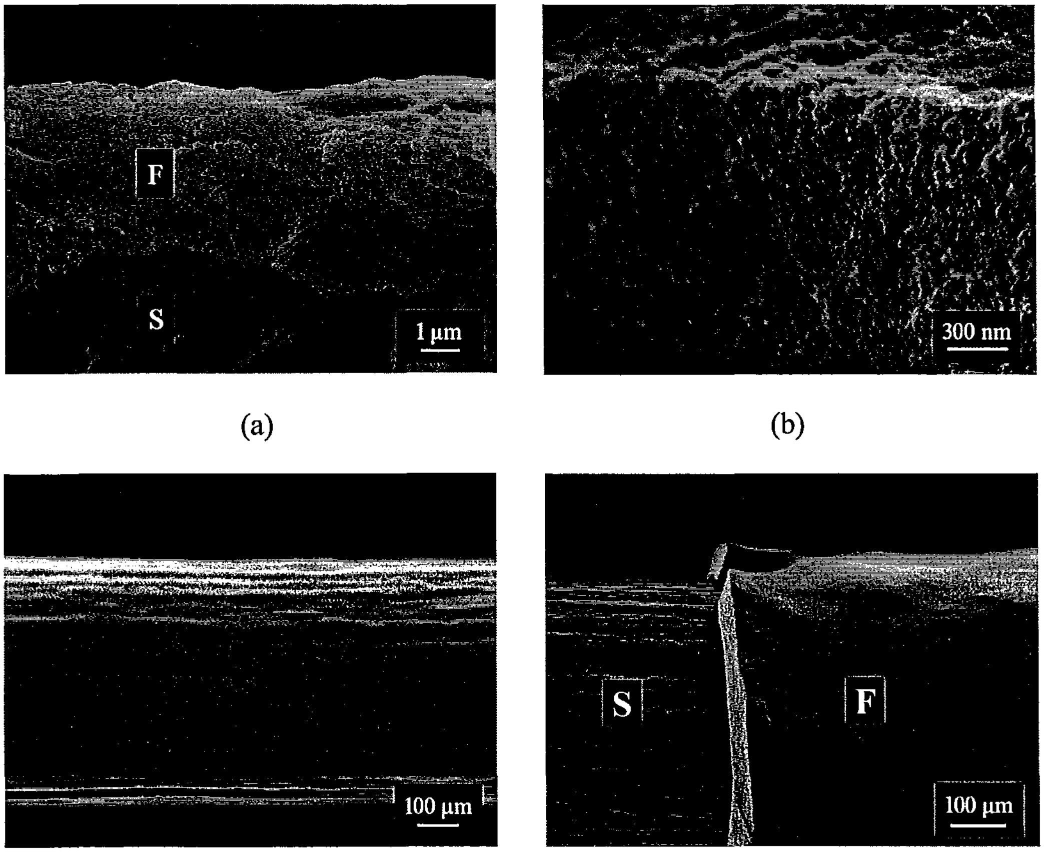

(a) (b)

(c) (d)

Figure 5-25 SEM images at different magnifications for deposits obtained from 3 g L^{-1} MnO_2 suspensions on (a and b) graphite and (c and d) graphite rods (F-deposit, S-substrate).

SEM investigations indicate that EPD can be used for the fabrication of manganese dioxide films on various conductive substrates. The possibility of deposition of porous films on substrates of complex shape is important for application of the films in ES. The films exhibited microporosity, which is important for the electrolyte access to the active material. On the other hand, the deposition on high surface area substrates such as stainless steel meshes is important for the reduction of electrical contact resistance[20].

5.4.3 Capacitive behavior studies of MnO_2 films

The mechanism of charge storage in manganese oxides is based on the adsorption of ions on the oxide surface. The pseudocapacitance of hydrous manganese dioxide is attributed to reversible redox transitions involving exchange of protons and/or cations with the electrolyte (Equation 2-10). The analysis of Equation 2-10 indicates that high ionic and electronic conductivity of the active material are necessary in order to achieve a high SC. The values of SC reported in the literature[3-5] for MnO_2 electrodes are usually in the range between 100 and 350 F g^{-1}. These values are far from the theoretical SC[2] of 1370 F g^{-1} and reported experimental SC of 700 F g^{-1} for very thin (4 μg cm^{-2}) films[51, 52]. The reduction in SC with increasing film thickness was attributed to low electronic conductivity of MnO_2.

The capacitive behavior of the films prepared by EPD was investigated in the potential range of 0-1.0 V versus SCE. Figure 5-26 shows typical CVs for the 50 μg

cm^{-2} sample in the 0.1 M Na_2SO_4 solutions. Within the potential range of 0-1.0 V versus SCE the manganese dioxide electrodes exhibited capacitive-like current–potential responses, as indicated by the box shape of the CVs. It is clear from Figure 5-26 that there are no redox peaks in the range between 0 and 1.0 V. The highest specific capacitance of 412 F g^{-1} was obtained at a scan rate of 2 mV s^{-1}. However, the SC decreased with increasing scan rate and increasing film thickness (Figure 5-27). Similar reduction in SC was observed in other investigations[51, 52, 82, 104] and was attributed to low electronic and ionic conductivity of the MnO_2 electrodes. The films prepared by EPD showed good cycling behavior with no loss in SC during 1000 cycles (Figure 5-28). Testing results indicated that EPD is a promising technique for the fabrication of electrodes for ES. Further improvement in the electrochemical properties of manganese dioxide films can be achieved by the use of conductive additives and modification of film composition and microstructure.

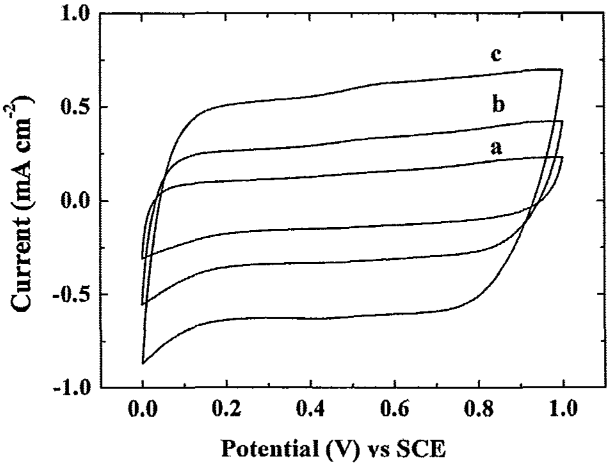

Figure 5-26 CVs for the 50 μg cm^{-2} film on a stainless steel substrate at scan rates of (a) 20 mV s^{-1}, (b) 50 mV s^{-1} and (c) 100 mV s^{-1} in the 0.1 M Na_2SO_4 solutions.

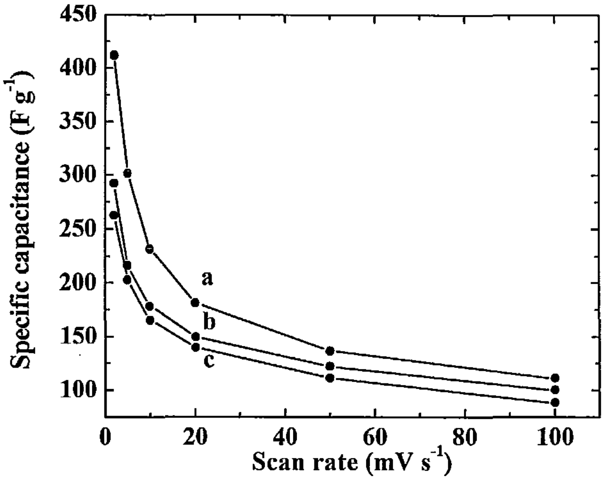

Figure 5-27 Specific capacitance versus scan rate for films of different mass: (a) 50 μg cm^{-2}, (b) 90 μg cm^{-2} and (c) 160 μg cm^{-2} tested in the 0.1 M Na_2SO_4 solutions.

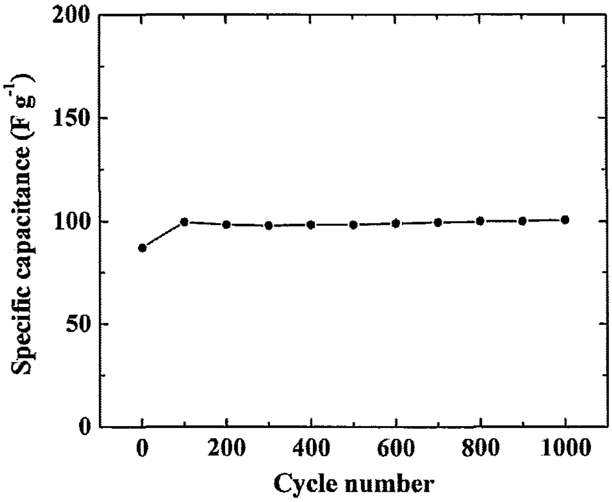

Figure 5-28 Specific capacitance for a 90 μg cm^{-2} film tested in the 0.1 M Na_2SO_4 solutions versus cycle number at a scan rate of 100 mV s^{-1}.

5.5 Anodic EPD of MnO_2/MWCNTs composites

As discussed in chapter 5.3.3, due to the low conductivity, the SC of MnO_2 nanofiber electrodes was far from the theoretical value. The SC decreased significantly with increasing scan rate. It was suggested that conductive additives, such as carbon black, can enhance the electronic conductivity of MnO_2 electrodes[50]. However, the SC of carbon additives is low and therefore the carbon additive content in the composite materials must be optimized. The use of carbon nanotubes as conductive additives has benefits of high surface area and low percolation threshold[105]. Therefore, the formation of composite electrodes containing manganese dioxide nanofibers and carbon nanotubes offers an advantage of improved contact between two different fibrous materials, lower binder and carbon content, which can result in improved electrochemical properties of the composite electrodes.

Hence, the co-deposition of MnO_2 and MWCNTs was conducted. It was found that sodium alginate polyelectrolyte was a common dispersant, charging additive and binder for both MnO_2 and MWCNTs, which can stabilize and charge MWCNTs in the MnO_2 suspensions. Obtained results indicated that adding MWCNTs in the films can improve the electrochemical behavior. The composite films exhibited higher SC and better CV windows and lower ERS than the MnO_2 films without MWCNTs.

5.5.1 SEM investigations of the composite deposits

Figure 5-29 showed SEM images of surface and cross-sections of the composite deposits. The SEM images of the surface at different magnifications showed that the deposits were crack free (Figure 5-29a) and exhibited porosity with typical pore size of 10-100 nm (Figure 5-29b). Cross-section images of the deposits of different thickness, prepared at different deposition times, indicated that obtained films were relatively uniform (Figure 5-29c and Figure 5-29d). The thickness of the deposits was varied in the range of 0-20 μm by variation of deposition time in the range of 1-10 min and deposition voltage in the range of 10-50 V. The high magnification images of the surface (Figure 5-29b) and cross-section (Figure 5-29e) indicated the composite nature of the deposits, which contained two different fibrous materials.

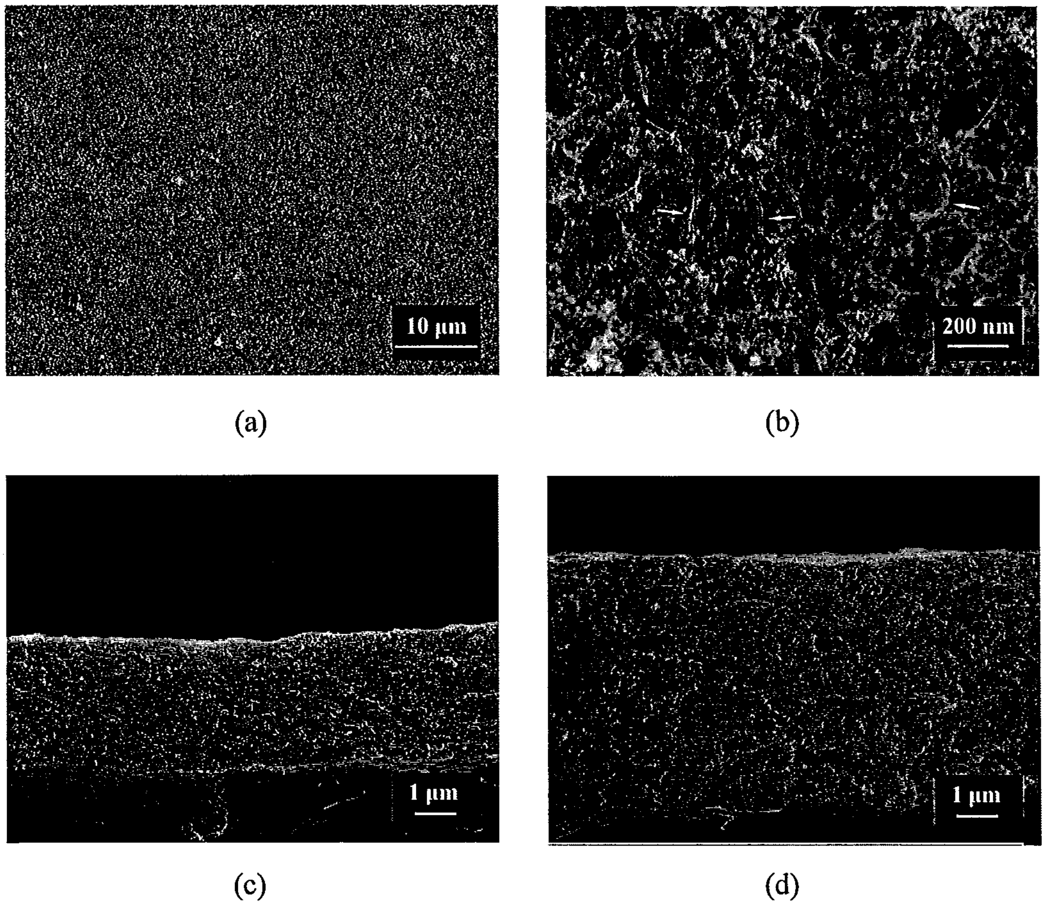

(a) (b)

(c) (d)

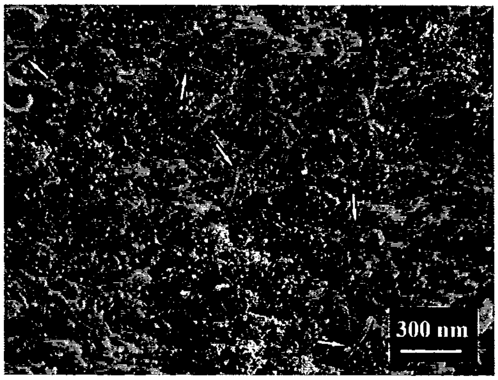

(e)

Figure 5-29 SEM images of the composite deposits prepared from the 0.1 g L^{-1} sodium alginate solution, containing 3.3 g L^{-1} MnO_2 and 0.1 g L^{-1} MWCNTs: (a and b) surface of the deposits on a stainless steel substrate at different magnifications, (c and d) cross-sections of the deposits of different thickness on graphite substrates and (e) high magnification image of a cross-section, arrows show MWCNTs, deposition voltage 15 V, deposition time 2 min (a–c) and 4 min (d and e).

5.5.2 TGA&DTA studies of the composite deposits

The deposits prepared by EPD were studied by TGA and DTA. The TGA data (Figure 5-30) showed higher weight loss for the deposits compared with that for as-prepared manganese dioxide nanofibers. The total weight loss at 1200 °C for the deposits prepared from the 0.1 g L^{-1} sodium alginate solutions, containing 3.3 g L^{-1} manganese dioxide was found to be 26.0 wt.%. The manganese dioxide nanofibers showed the total weight loss of 20.3 wt.%. The difference of 5.7 wt.% was attributed to burning out of alginic acid and indicated the codeposition of alginic acid and manganese dioxide. It should be noted that the small weight gain related to the oxidation of non-stoichiometric manganese dioxide was not observed in the TGA data for the composite deposit due to the weight loss related to burning out of the organic phase.

The exotherm in the DTA data for the composite deposit at 500 °C (Figure 5-31) can be attributed to the oxidation of the non-stoichiometric manganese dioxide and burning out of the alginic acid. It is important to note that polymer binders are usually added to EPD suspensions in order to increase the adherence and strength of the deposited materials and prevent cracking. The results of TGA analysis indicate that alginic acid polymer is included in the deposits. Therefore, binding properties of alginic acid[106] can be utilized in the fabrication of manganese dioxide films by EPD.

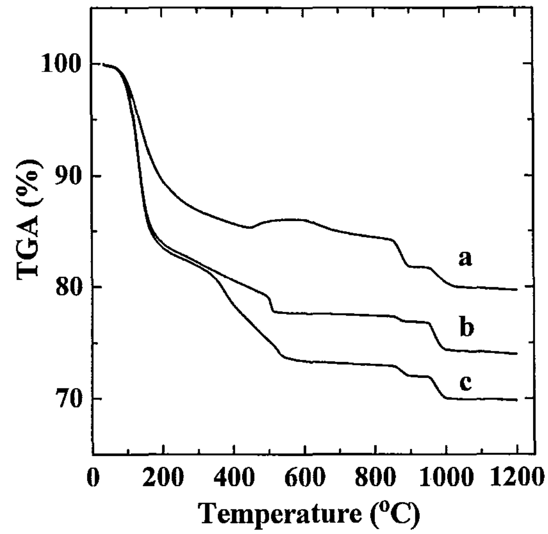

Figure 5-30 TGA data for (a) as-prepared MnO_2 nanofibers, (b) the deposit prepared from the 0.1 g/L sodium alginate solution, containing 3.3 g L^{-1} MnO_2 and (c) the deposit prepared from the 0.1 g/L sodium alginate solution, containing 3.3 g L^{-1} MnO_2 and 0.1 g L^{-1} MWCNTs, deposition voltage 15 V (b and c).

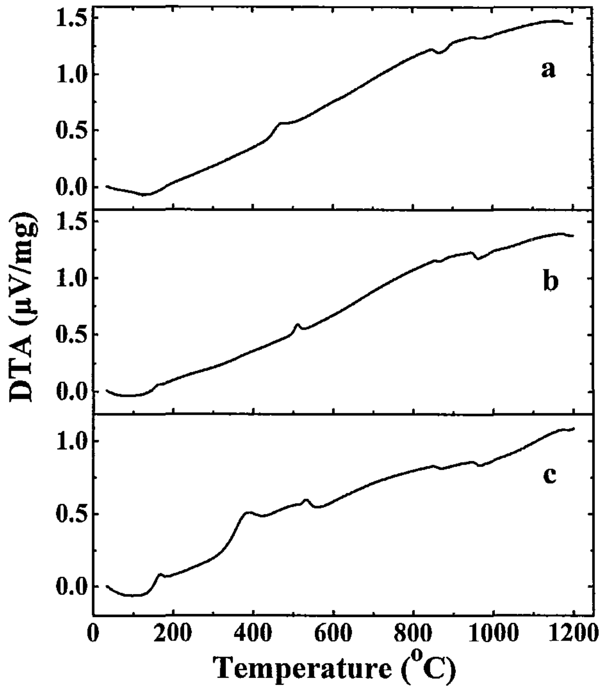

Figure5-31 DTA data for (a) as-prepared MnO_2 nanofibers, (b) the deposit prepared from the 0.1 g L^{-1} sodium alginate solution, containing 3.3 g L^{-1} MnO_2 and (c) the deposit prepared from the 0.1 g L^{-1} sodium alginate solution, containing 3.3 g L^{-1} MnO_2 and 0.1 g L^{-1} MWCNTs, deposition voltage 15 V (b and c).

Sodium alginate was found to be an effective additive for the dispersion and charging of MWCNTs. Composite alginic acid-MWCNTs films were obtained by EPD. Figure 5-32 and Figure 5-33 compare TGA and DTA data for the deposits prepared from the 0.5 g L^{-1} sodium alginate solutions, as-received MWCNTs and deposits prepared from the 0.5 g L^{-1} sodium alginate solutions, containing 0.05 g L^{-1} carbon nanotubes.

The TGA and DTA data for alginic acid showed the weight loss below 475 °C (Figure 5-32) and a broad exotherms in the range of 300-500 °C (Figure 5-33) related to burning out of alginic acid. The weight of MWCNTs sample was relatively stable at temperatures below 500 °C (Figure 5-32). A sharp reduction of the sample weight in the range of 500-680 °C (Figure 5-32) and broad exotherms (Figure 5-33) in the same range are related to burning out of MWCNTs. The TGA data (Figure 5-32) for the deposit prepared from the 0.5 g L^{-1} sodium alginate solutions, containing 0.05 g L^{-1} carbon nanotubes, showed significant reduction in the sample weight below 400 °C and the additional weight loss step in the range of 550-600 °C. The DTA data (Figure 5-33) showed two corresponding exotherms around 350 and 550 °C. It is suggested that two steps in the weight loss and two corresponding exotherms are related to burning out of alginic acid and MWCNTs, indicating the formation of composite alginic acid-MWCNTs deposits. The TGA and DTA data showed that the thermal degradation of the composite sample was achieved at lower temperatures, compared to pure MWCNTs. It is suggested that that burning out of alginic acid promoted the thermal degradation of MWCNTs at reduced temperatures.

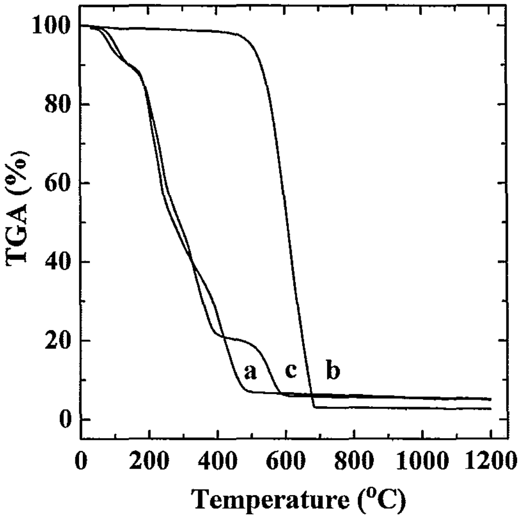

Figure 5-32 TGA data for (a) the deposit prepared from the 0.5 g L^{-1} sodium alginate solution, (b) as-received MWCNTs and (c) the deposit prepared from the 0.5 g L^{-1} sodium alginate solution, containing 0.05 g L^{-1} MWCNTs, deposition voltage 15 V (a and c).

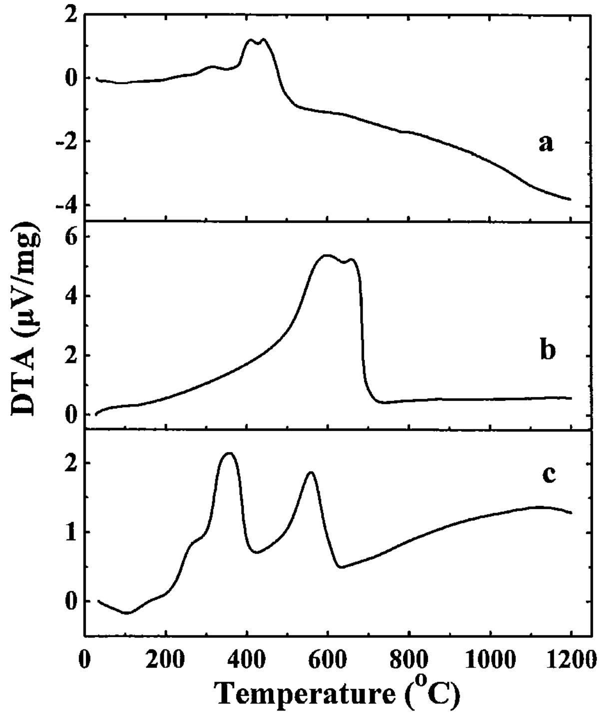

Figure 5-33 DTA data for (a) the deposit prepared from the 0.5 g L^{-1} sodium alginate solution, (b) as-received MWCNTs and (c) the deposit prepared from the 0.5 g L^{-1} sodium alginate solution, containing 0.05 g L^{-1} MWCNTs, deposition voltage 15 V (a and c).

Obtained results indicate that alginate can be used as a dispersant, charging additive and a binder for EPD of two different fibrous materials: manganese dioxide nanofibers and MWCNTs. Therefore, alginate can be used for codeposition of manganese dioxide nanofibers and MWCNTs. Figure 5-30 compares TGA data for the deposits prepared from the 0.1 g L^{-1} sodium alginate solutions, containing 3.3 g L^{-1} manganese dioxide without nanotubes and containing 0.1 g L^{-1} carbon nanotubes. The deposit, prepared from the suspension containing MWCNTs showed total weight loss of 30.2 wt.%, which is higher than the weight loss of the sample (26.0 wt.%) prepared from the suspension without MWCNTs. The difference can be attributed to burning out of MWCNTs. The corresponding DTA data (Figure 5-31) showed the additional broad exotherm in the range of 350-550 °C.

The comparison of the TGA data (Figure 5-30) for as-prepared manganese dioxide nanofibers and deposits indicates that the deposits prepared from the 0.1 g L^{-1} sodium alginate solutions, containing 3.3 g L^{-1} manganese dioxide and 0.1 g L^{-1} MWCNTs are composites, containing manganese dioxide, 6 wt.% of binder and 4 wt.% of MWCNTs.

5.5.3 Electrochemical characterization of composite films

Figure 5-34 shows typical CVs for the composite deposit at different scan rates. Within the potential range of 0-1.0 V versus SCE the composite electrode exhibited capacitive-like current-potential response, indicated by the box shape of the CVs. SC calculated from the CV data decreased with increasing scan rate (Figure 5-35). Higher SC was observed for the deposits containing MWCNTs compared to the sample of the same mass without MWCNTs. The addition of MWCNTs resulted in larger area and improved box shape of the CV windows (Figure 5-35, insert). This can be attributed to the higher conductivity of the deposits, containing MWCNTs. The SC decreased with increasing sample mass (Figure 5-36). The decrease in SC with increasing scan rate and increasing sample thickness can be attributed to the diffusion limitations in pores and the low conductivity of the composite electrodes[20].

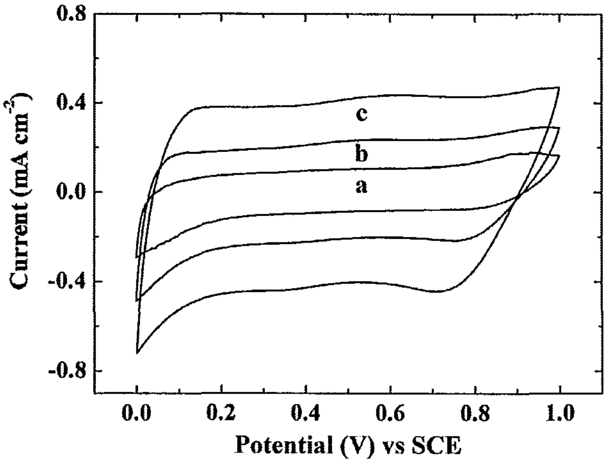

Figure 5-34 CVs for the 0.24 mg cm^{-2} deposit prepared from the 0.1 g L^{-1} sodium alginate solution, containing 3.3 g L^{-1} MnO_2 and 0.1 g L^{-1} MWCNTs at scan rates of (a) 2 mV s^{-1}, (b) 5 mV s^{-1} and (c) 10 mV s^{-1}, deposition voltage 15 V.

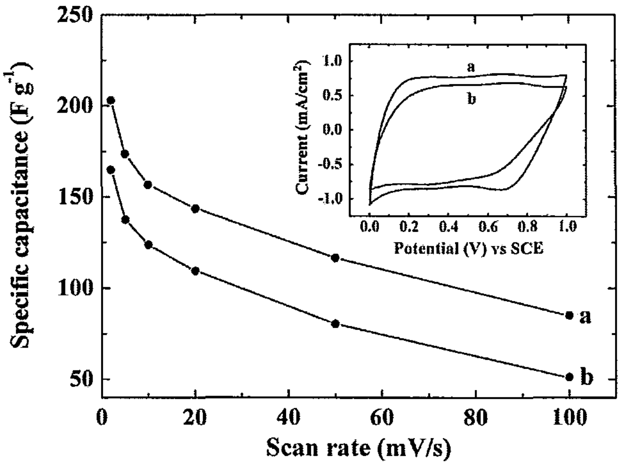

Figure 5-35 Specific capacitance versus scan rate for the 0.24 mg cm^{-2} deposits and corresponding CVs (insert) at a scan rate of 20 mV s^{-1} for (a) the deposit prepared from the 0.1 g L^{-1} sodium alginate solution, containing 3.3 g L^{-1} MnO_2 and 0.1 g L^{-1} MWCNTs and (b) the deposit prepared from the 0.1 g L^{-1} sodium alginate solution, containing 3.3 g L^{-1} MnO_2 without MWCNTs, deposition voltage 15 V.

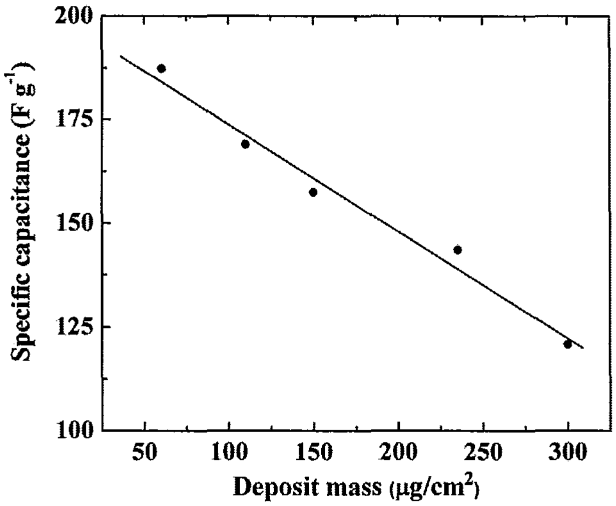

Figure 5-36 Specific capacitance at a scan rate of 20 mV s^{-1} versus deposit mass for the deposits prepared from the 0.1 g L^{-1} sodium alginate solution, containing 3.3 g L^{-1} MnO_2 and 0.1 g L^{-1} MWCNTs, deposition voltage 15 V.

Figure 5-37 shows impedance data for the MnO_2 and composite films. The value of the real part of complex impedance at high frequency can be used for the estimation of equivalent series resistance. The composite films have much lower ESR, indicating that the addition of MWCNTs can reduce the resistance of the films. The impedance obtained at the highest frequency is mainly attributed to the deposit resistance[20].

It is important to note that obtained SC values for manganese dioxide electrodes fabricated by EPD are comparable with literature data for SC of manganese electrodes of similar mass prepared by other methods[5]. It is expected that further optimization of the deposit composition, microstructure and processing conditions will result in improved performance of the electrodes prepared by EPD. Therefore, EPD is a promising method for the fabrication of electrodes for ES.

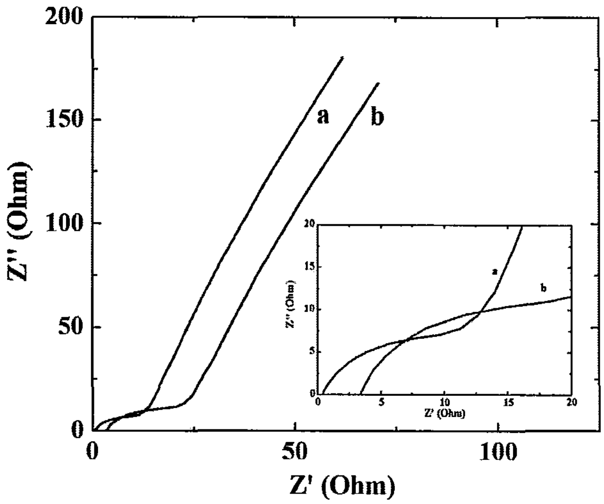

Figure 5-37 Impedance data for the 0.24 mg cm^{-2} deposits for (a) the deposit prepared from the 0.1 g L^{-1} sodium alginate solution, containing 3.3 g L^{-1} MnO_2 and 0.1 g L^{-1} MWCNTs and (b) the deposit prepared from the 0.1 g L^{-1} sodium alginate solution, containing 3.3 g L^{-1} MnO_2 without MWCNTs, (insert shows impedance data in the high frequency range), deposition voltage 15 V.

5.6 Cathodic EPD of MnO_2 nanofibers

EPD is an important technique for the deposition of nanostructured films[78, 79]. In addition to anodic EPD techniques discussed above, cathodic EPD is another approach to fabricate manganese dioxide films[78]. It offers important advantages compared to the anodic EPD. In this procedure, the problem related to the anodic oxidation of high surface area current collectors can be avoided. However, cathodic EPD of MnO_2 films presents difficulties due to the lack of effective charging additives and dispersants for charging and dispersion of MnO_2. In our cathodic EPD method, it was found that phosphate ester is an effective charging additive, which provides stabilization of MnO_2 nanoparticles in suspensions. In this work the feasibility of cathodic EPD of MnO_2 films has been demonstrated. The deposition mechanism has been developed and kinetics of deposition has been investigated.

5.6.1 Deposition yield

It was found that the suspensions of manganese dioxide in ethanol were unstable and showed sedimentation when ultrasound treatment was interrupted (Figure 5-38, insert a). The cathodic deposits obtained from such suspensions were highly agglomerated and non-uniform. In contrast, relatively uniform deposits were obtained from well dispersed and stable suspensions of manganese dioxide containing phosphate ester as a dispersant(Figure 5-38, insert b). Figure 5-38 shows a typical dependence of the deposition yield on PE concentration. The deposition rate increased with increasing PE concentration showing a maximum and decreased at higher PE concentrations.

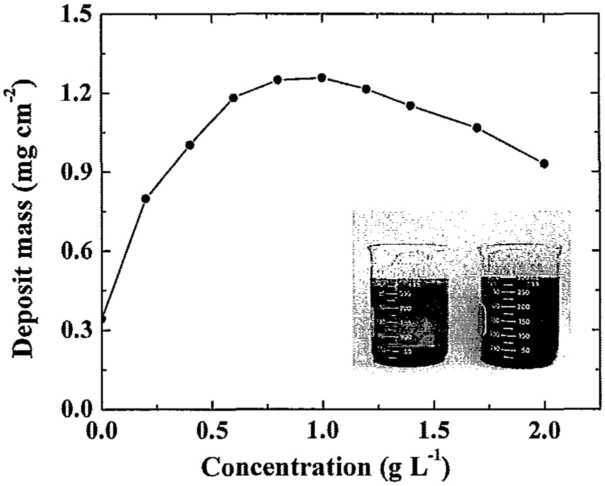

Figure 5-38 Deposit mass for films on stainless steel substrates versus phosphate ester concentration in the 45 g L^{-1} manganese dioxide suspensions at a deposition voltage of 20 V and deposition time of 1 min. Insert shows suspensions (a) without PE, one day after ultrasonic treatment and (b) containing 1 g L^{-1} PE, 7 days after ultrasonic treatment.

The formation of cathodic deposits indicated that manganese dioxide particles were positively charged in ethanol suspensions. It is known that alcohols behave as proton donors[69, 72]. Pure alcohols can ionize in the following way:

$$RCH_2OH + RCH_2OH \rightarrow RCH_2O^- + RCH_2O_2^+ \qquad (5\text{-}4)$$

Damodaran and Moudgil[72] have proposed a mechanism of particle charging, in which the adsorbed alcohol ionized into a protonated alcohol and an alkoxide ion, followed by the dissociation of the protonated alcohol. The dissociated alcohol and alkoxide ion desorbed into the solution, leaving a proton on the particle surface.

It is suggested that the addition of phosphate ester to the suspensions resulted in electrostatic stabilization[69] of the manganese dioxide nanoparticles. It is known that phosphate ester is an effective electrostatic stabilizer[69], which charges oxide particles positively in organic liquids by donating protons to the surface. Moreover, phosphate ester acts as a steric dispersant by anchoring the long-chain molecules to the particle surfaces.

The increasing deposition yield in the range of 0-1 g L^{-1} can be attributed to improved suspension stability and increasing charge of the manganese dioxide nanoparticles. It is suggested that further addition of PE increased the ionic strength of the suspensions, resulting in a reduced thickness of the electrical double layer of manganese dioxide particles and lower suspension stability. The lower suspension stability and particle sedimentation lead to the reduction in the suspension concentration and lower deposition rate. As a result, the deposition yield versus PE concentration dependence showed a maximum. Similar dependences were observed for other oxide materials[107]. The deposition rate in the EPD process can be described by Hamaker equation (Equation 5-1), which predicts an increase in the deposit mass M with increasing deposition time t and suspension concentration C. The results of this investigation showed that the problem of low colloidal stability of manganese dioxide suspensions can be addressed by the use of PE as a dispersant. It is known that the fabrication of stable suspensions of manganese dioxide with particle concentration above 1 mM presents difficulties[104]. The dilute suspensions with particle concentration below 1 mM cannot be used for practical applications of EPD. It is in this regard that the deposition rate in the EPD process is proportional to particle concentration in the suspensions (Equation 5-1). The use of PE enabled the formation of concentrated suspensions of charged manganese dioxide particles and relatively high deposition yield was obtained, which was comparable with the deposition yield reported in the EPD literature for other materials[69, 108].

The deposit mass (Figure 5-39) increased with increasing deposition time in agreement with Equation 5-1. The deposit mass versus deposition voltage dependence was non-linear (Figure 5-40), and can not be explained by the Hamaker equation. The increase in the slope of this dependence at low voltages can be attributed to the orientation of nanofibers in the suspensions during deposition. The mechanism was similar to the orientation of carbon nanotubes, which was already discussed in the chapter 5.3.1.

The deposit yield measurements indicate that the amount of the deposited material can be varied by variation of the deposition time, voltage, concentration of phosphate ester and manganese dioxide in the suspensions. This is in a good agreement with the results of SEM investigations, which showed the formation of deposits of different thickness.

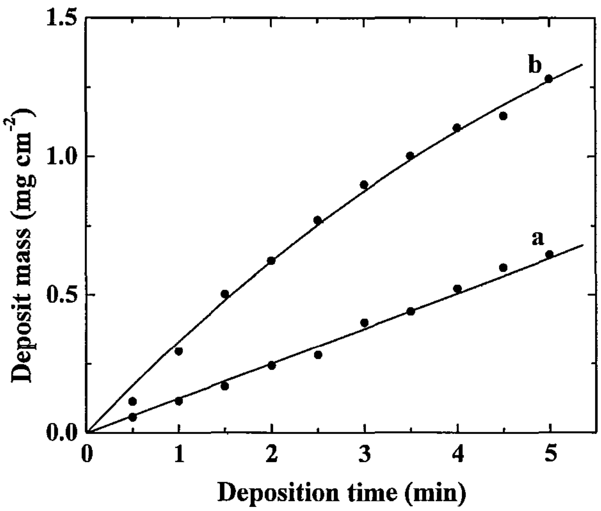

Figure 5-39 Deposit mass versus deposition time for films on stainless steel substrates obtained from 10 g L^{-1} MnO$_2$ suspensions, containing 1 g L^{-1} phosphate ester, at deposition voltages of (a) 10 V and (b) 20 V.

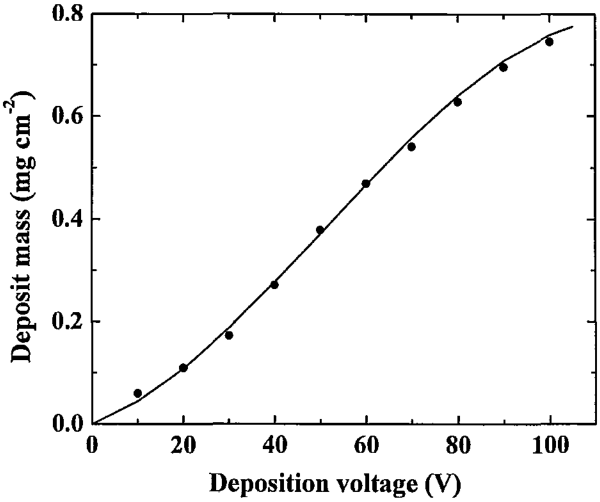

Figure 5-40 Deposit mass versus deposition voltage for films on stainless steel substrates obtained from 10 g L^{-1} MnO$_2$ suspensions, containing 0.2 g L^{-1} phosphate ester, at deposition time of 0.5 min.

5.6.2 SEM investigations of deposits

Figure 5-41 show typical SEM images of the deposits. SEM images of the surfaces indicated that the deposits were crack free and exhibited porosity with a pore size of about 10-100 nm (Figure 5-41a). The deposition process resulted in the formation of relatively uniform deposits (Figure 5-41b) with thickness in the range of 0.5-20 μm. The deposits consisted of nanofibers. The fibrous microstructure of the deposits is in a good agreement with TEM and SEM investigations of individual particles. It is important to note that film porosity is beneficial for crack prevention in thick films owing to crack tip blunting mechanism[109]. Moreover, film porosity and small size of nanofibers were beneficial for application in ES.

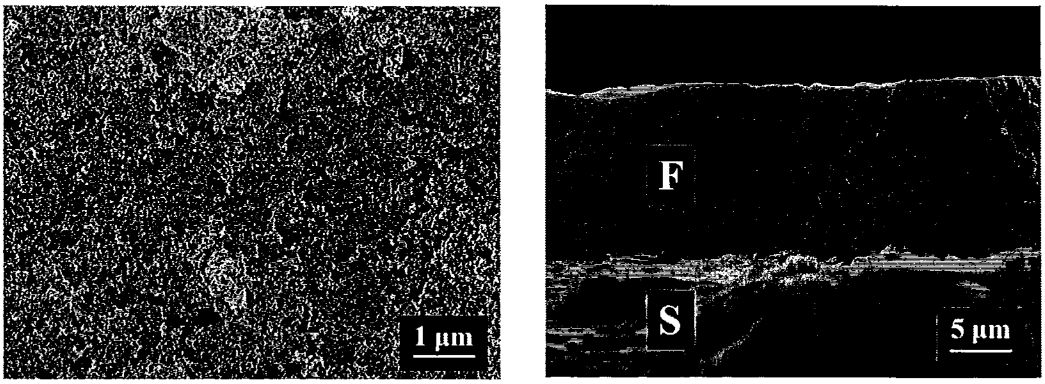

(a) (b)

Figure 5-41 SEM images of a film on a stainless steel substrate (a) and film fracture on a graphite substrate (b), prepared from 10 g L^{-1} MnO_2 suspension, containing 0.2 g L^{-1} phosphate ester at a deposition voltage of 20 V. (F-deposit, S-substrate).

5.6.3 Capacitive behavior studies of MnO_2 films

The porous electrophoretic deposits containing manganese dioxide nanofibers showed good capacitive behavior in the 0.1 M Na_2SO_4 aqueous electrolyte. Figure 5-42 shows typical CVs in the 0.1 M Na_2SO_4 solutions obtained at different scan rates in the potential range of 0-1.0 V versus SCE. The manganese dioxide electrodes exhibited capacitive-like current-potential response. It is clear from Figure 5-42 that there are no redox peaks in the range between 0 and 1.0 V.

The SC of the obtained films was calculated from the CV curves using Equation 4-2. The results presented in Figure 5-43 indicated that SC measured at a scan rate of 2 mV s^{-1} was 377, 301, 277 and 223 F g^{-1} for film mass of 50, 90, 130 and 170 μg cm^{-2}, respectively. The decrease in SC with increasing film mass and increasing scan rate can be attributed to the low electronic and ionic conductivity of manganese dioxide. It is important to note that the SC of manganese dioxide films of similar mass prepared by other methods[74, 94] was in the range of 150-300 F g^{-1}. Therefore cathodic EPD is a promising method for the fabrication of manganese dioxide films for ES.

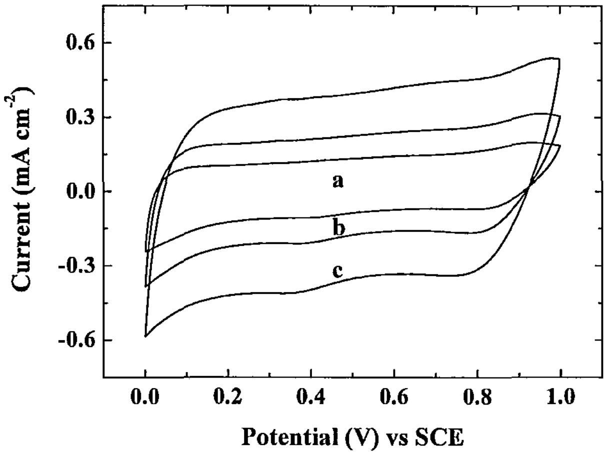

Figure 5-42 CVs for the 90 μg cm^{-2} film on a stainless steel substrate at scan rates of (a) 2 mV s^{-1}, (b) 5 mV s^{-1} and (c) 10 mV s^{-1} in the 0.1 M Na_2SO_4 solution.

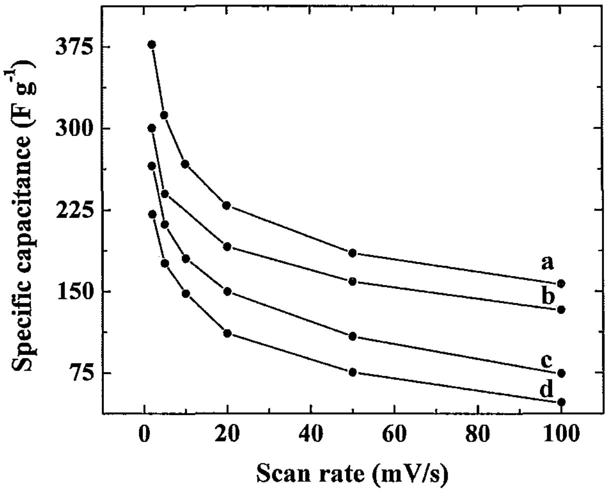

Figure 5-43 Specific capacitance versus scan rate for films of different mass on stainless steel substrates: (a) 50 μg cm^{-2}, (b) 90 μg cm^{-2}, (c) 130 μg cm^{-2} and (d) 170 μg cm^{-2} tested in the 0.1 M Na_2SO_4 solutions.

5.6.4 Impedance spectroscopy and chronopotentiometry studies

Figure 5-44 shows charge/discharge behavior of manganese dioxide film in the 0.1 M Na_2SO_4 solution. The charge and discharge curves are almost linear and indicate good capacitive behavior in agreement with the CV data. The small initial potential drop observed during discharge can be attributed to the low conductivity of the active material and electrolyte diffusion limitations. According to Equation 4-4 and Equation 4-5, for the 130 $\mu g\ cm^{-2}$ MnO_2 film, a power density of 1.92 $kW\ kg^{-1}$ was obtained at an energy density of 27.73 $Wh\ kg^{-1}$.

The films were studied by the impedance spectroscopy method (Figure 5-45). The equivalent circuit used for data analysis included R_nQ_n transmission line describing the porous electrodes and solution resistance (R_s)[97, 98]. R_n elements represented electrolyte resistance in pores, Faradaic resistance and equivalent series resistance of the electrodes[98]. The constant phase elements CPE (Q) described capacitors with microscopic roughness of the surface and capacitance dispersion of interfacial origin[98]. Good agreement of simulated and measured impedance data was found for the equivalent circuit containing a transmission line with 3 RQ elements. The high frequency Z' value of the complex impedance $Z=Z'-iZ''$ showed that total resistance[20] is about 1 Ohm for the sample area of 1 cm^2.

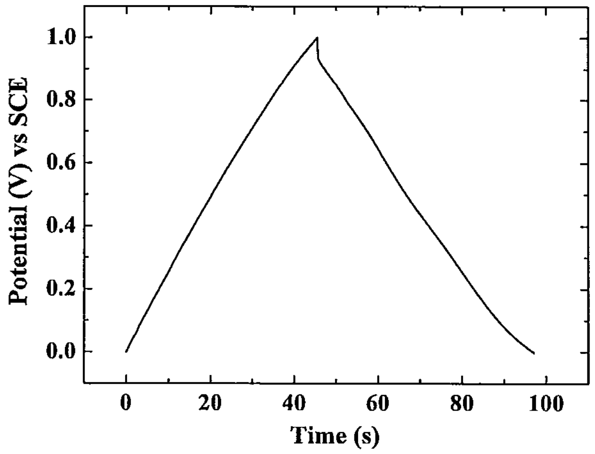

Figure 5-44 Chronopotentiometry data at a current density of 0.5 mA cm^{-2} for the 130 μg cm^{-2} film on a stainless steel substrate in the 0.1 M Na_2SO_4 solution.

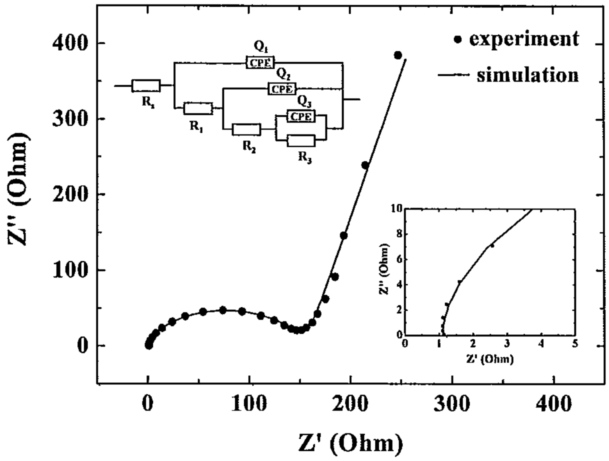

Figure 5-45 Impedance spectroscopy data for 400 μg cm^{-2} film on a stainless steel substrate in the 0.1 M Na_2SO_4 solution. Inserts show the data in the high frequency range and equivalent circuit.

Obtained results indicate that EPD is a promising method for the fabrication of ES. It is in this regard that microstructure of the electrode materials is an important factor, determining ES performance. The development of ES requires the use of electrodes with small particle size, high surface area and high porosity, which allow good electrolyte access to the active material. The traditional approach of impregnation and pressing can result in reduced porosity, increased resistance and decreased SC. In contrast, EPD from colloidal solutions enables the deposition of porous nanostructured electrode materials on current collectors. Compared to other deposition techniques, such as electrodeposition and sol-gel method, EPD offers the advantages of higher deposition rate and the possibility of the fabrication of thick coatings[69]. It is suggested that further development of the EPD method will result in improved capacitive behavior and reduced electrode resistance. This can be achieved by the EPD of porous composite materials, containing manganese dioxide, cathodic co-deposition of MnO_2 and carbon nanotubes on the current collectors with complex shape and high surface area.

Chapter 6 Conclusions

New method has been developed for the fabrication of manganese dioxide nanofibers. The method is simple, low cost and suitable for mass production. Manganese dioxide nanofibers have been prepared by a chemical precipitation method. The precipitation was performed by the reduction of 0.2 M $KMnO_4$ solutions with ethanol. As-prepared nanofibers with length ranged from 0.1 to 1 μm and diameter of 3-10 nm showed low crystallinity and contained adsorbed water. EDS studies showed that as-prepared material contained K and Mn species. It was found that the reaction time can affect the morphology of manganese dioxide nanoparticles. When the reaction time was prolonged, the individual nanofibers started to agglomerate to form nanobundles.

Composite electrodes containing two different fibrous materials were fabricated by impregnation of slurries of manganese dioxide nanofibers and MWCNTs into porous nickel foam and plaque current collectors. MWCNTs improved electrochemical performance of the electrodes by forming a secondary conductivity network within the porous nickel structures. The nickel foam based composite electrodes with total mass loading of 40 mg cm^{-2} showed a capacitive behavior in the 0.1-0.5 M Na_2SO_4 solutions. Testing in the 0.5 M Na_2SO_4 solutions showed higher SC compared to the SC in the 0.1 M Na_2SO_4 solutions. The SC increased with increasing MWCNTs content in the range of 0-20 wt.%, showing more distinct effect at higher scan rates, and decreased with increasing scan rate. The highest SC of 155 F g^{-1} was obtained at a scan rate of 2 mV s^{-1} in the 0.5 M Na_2SO_4 solutions.

The nickel plaque based composite electrodes with total mass loading of 7-15 mg cm^{-2} showed good capacitive behavior in the 0.5 M Na_2SO_4 solutions. The reduction of stirring time of the precipitated nanofibers resulted in lower agglomeration and higher SC. The highest SC of 185 F g^{-1} was obtained at a scan rate of 2 mV s^{-1} for materials loading of 7 mg cm^{-2}.

Anodic EPD has been developed using sodium alginate polyelectrolyte as a dispersant and charging additive. Stable high concentration suspensions of manganese dioxide were obtained. The feasibility of EPD of manganese dioxide nanofibers has been demonstrated. Nanostructured films have been deposited on various conductive substrates of complex shape and exhibited a fibrous porous microstructure with a pore size in the range of 10-50 nm. The film thickness was varied from 2 to 100 μm by the variation in deposition voltage in the range of 5-50 V and deposition time in the range of 1-10 min. The films showed good capacitive behavior with a box shape CV in the range of 0-1.0 V in the 0.1 M Na_2SO_4 solutions. The highest specific capacitance of 412 F g^{-1} was obtained at a scan rate of 2 mV s^{-1}. The capacitance decreased with increasing scan rate and increasing film thickness. Good cycling behavior was observed for the films, with no loss in SC during 1000 cycles.

Anodic EPD of manganese dioxide and MWCNTs were achieved using sodium alginate polyelectrolyte as a common dispersant, charging additive and binder. The composite films containing manganese dioxide and MWCNTs showed higher SC and lower ESR compared to the pure manganese dioxide films without MWCNTs. The SC decreased with increasing scan rate and increasing film thickness.

Cathodic EPD method has been developed for the deposition of manganese dioxide films. Stable suspensions of manganese dioxide for cathodic deposition were obtained using phosphate ester as a dispersant. It was shown that phosphate ester is an effective charging additive, which enables high deposition rate from 5-50 g L^{-1} manganese dioxide suspensions. The deposition yield can be varied by variation in manganese dioxide and phosphate ester concentration, deposition voltage and deposition time. The thickness of the films was in the range of 0.5-20 μm. The films electrochemically tested in the 0.1 M Na_2SO_4 solutions showed the pseudocapacitive behavior in a potential window of 1 V. The highest specific capacitance of ~ 377 F g^{-1} was obtained at a scan rate of 2 mV s^{-1}. The capacitance decreased with increasing film mass and increasing scan rate.

The electrodes prepared by impregnation techniques and EPD showed good capacitive performance and could be considered as possible electrodes for ES. Obtained results paved the way for the fabrication of advanced electrodes for supercapacitors.

References

1. B.E. Conway, *Electrochemical Supercapacitors - Scientific Fundamentals and Technological Applications.* 1999, New York: Kluwer.
2. S. Devaraj and N. Munichandraiah, *'High capacitance of electrodeposited MnO_2 by the effect of a surface-active agent'*, Electrochemical and Solid-State Letters, **8** (2005): pA373.
3. M. Toupin, T. Brousse and D. Belanger, *'Influence of microstructure on the charge storage properties of chemically synthesized manganese dioxide'*, Chemistry of Materials, **14** (2002): p3946.
4. C. Ye, Z.M. Lin and S.Z. Hui, *'Electrochemical and capacitance properties of rod-shaped MnO_2 for supercapacitor'*, Journal of the Electrochemical Society, **152** (2005): pA1272.
5. R.N. Reddy and R.G. Reddy, *'Sol-gel MnO_2 as an electrode material for electrochemical capacitors'*, Journal of Power Sources, **124** (2003): p330.
6. H.E. Becker, U.S.,Patent 2 800 616, General Electric, (1957).
7. D.I. Boss, U.S., Patent 3 536 963, Standard Oil, SOHIO, (1970).
8. X. Andrieu, *'Ultracapacitors for portable electronics'*, Energy Storage Systems for Electronics: New Trends in Electrochemical Technology, **1** (2000): p521.
9. S. Hadzi-Jordanov, H. Angerstein-Kozlowska, M. Vukovic and B.E. Conway, *'Reversibility and growth behavior of surface oxide films at ruthenium electrodes'*, Journal of the Electrochemical Society, **125** (1978): p1471.
10. S. Trasatti and G. Buzzanca, *'Ruthenium dioxide: A new interesting electrode material. Solid state structure and electrochemical behaviour'*, Journal of Electroanalytical Chemistry, **29** (1971): pA1.
11. D. Galizzioli, F. Tantardini and S. Trasatti, *'Ruthenium dioxide: A new electrode material em dash 2. non-stoichiometry and energetics of electrode reactions in acid solutions "*, Journal of Applied Electrochemistry, **5** (1975): p203.
12. T.C. Murphy, R.B. Wright, R.A. Sutula, in: F.M. Delnick, D. Ingersoll, X. Andrieu, K. Naoi (Eds.), Electrochemical Capacitors II, Proceedings, vols. 96-25, The Electrochemical Society, Pennington, NJ, 1997, P.258.
13. R.J. Brodd, K.R. Bullock, R.A. Leising, R.L. Middaugh, J.R. Miller and E. Takeuchi, *'Batteries, 1977 to 2002'*, Journal of the Electrochemical Society, **151** (2004): pK1.
14. I. N. Varakin, A. D. Klementov, S. V. Litvinenko, N. F. Starodubtsev, and A. B. Stepanov, in Proceedings of 7th International Seminar on Double Layer Capacitors and Similar Energy Storage Devices, Deerfield Beach, FL, 1997.
15. S. Razuomov, A. Klementov, S. Litinenko and A. Beliakov, U.S. Patent 6 222 723, (2001).
16. J. Schindall, *'The Charge of the Ultra-Capacitors'*, Spectrum, IEEE, **44** (2007): p42.
17. J.P. Zheng, J. Huang and T.R. Jow, *'The limitations of energy density for electrochemical capacitors'*, Journal of the Electrochemical Society, **144** (1997): p2026.
18. A.K. Shukla, S. Sampath and K. Viayamohanan, *'Electrochemical Supercapacitors: Energy Storage Beyond Batteries'*, Current Science, **79** (2000): p1656.
19. T. R. Jow and J. P. Zheng, in Electrochemical Capacitors, F, M. Delnick, D. Ingersoll, X.

Andrieu, K. Naui, Editors, PV 96-25, p. 26, The Electrochemical Society Proceedings Series, Perinington, NJ (1997).

20. R. Kötz and M. Carlen, *'Principles and applications of electrochemical capacitors'*, Electrochimica Acta, **45** (2000): p2483.
21. J.R. Miller and A.F. Burke, *'Electrochemical capacitors:challenges and cpportunities for ceal-world applications'*, The Electrochemical Society Interface, **17** (2008): p53.
22. J.R. Miller and P. Simon, *'Fundamentals of electrochemical capacitor design and operation'*, The Electrochemical Society Interface, **17** (2008): p31.
23. J.W. Long, *'Electrochemical capacitors empowering the 21st century'*, The Electrochemical Society Interface, **17** (2008): p33.
24. C. Peng, S. Zheng, D. Jewell and G.Z. Chen, *'Carbon nanotube and conducting polymer composites for supercapacitors'*, Progress in Natural science, **18** (2008): p777.
25. E. Frackowiak and F. Béguin, *'Carbon materials for the electrochemical storage of energy in capacitors'*, Carbon, **39** (2001): p937.
26. A.G. Pandolfo and A.F. Hollenkamp, *'Carbon properties and their role in supercapacitors'*, Journal of Power Sources, **157** (2006): p14.
27. S. Iijima, *'Helical microtubules of graphite carbon'*, Nature, **354** (1991): p56.
28. S. Iijima and T. Ichihashi, *'Single-shell carbon nanotubes of 1-nm diameter'*, Nature, **363** (1993): p603.
29. C. Liu and H.-M. Cheng, *'Carbon nanotubes for clean energy applications'*, Journal of Physics D: Applied Physics, **38** (2005): pR231.
30. E.T. Thoteson, Z. Ren and T.-W. Chou, *'Advances in the science and technology of carbon nanotubes and their composites: a review'*, Composites Science and Technology, **61** (2001): p1899.
31. P.G. Collins and P. Avouris, *'Nanotubes for electronics'*, Scientific American, **293** (2000): p62.
32. M. Paradise and T. Goswami, *'Carbon nanotubes - Production and industrial applications'*, *Materials and Design*, **28** (2007): p1477.
33. C. Du and N. Pan, *'High power density supercapacitor electrodes of carbon nanotube films by electrophoretic deposition'*, Nanotechnology, **17** (2006): p5316.
34. E. Frackowiak, K. Metenier and V. Bertagna, *'Supercapacitor electrodes from multiwalled carbon nanotubes'*, Applied Physics Letters, **77** (2000): p2421.
35. E. Frackowiak, K. Jurewicz, S. Delpeux and F. Béguin, *'Nanotubular materials for supercapacitors'*, Journal of Power Sources, **97** (2001): p822.
36. K.H. An, K.K. Jeon, W.S. Kim, Y.S. Park, S.C. Lim, D.J. Bae and Y.H. Lee, *'Characterization of supercapacitors using single-walled carbon nanotube electrodes'*, Journal of the Korean Physical Society, **39** (2001): pS511.
37. B.-J. Yoon, S.-H. Jeong, K.-H. Lee, H.S. Kim, C.G. Park and J.H. Han, *'Electrical properties of electrical double layer capacitors with integrated carbon nanotube electrodes'*, Chemical Physics Letters, **388** (2004): p170.
38. E. Frackowiak, K. Jurewicz, K. Szostak, S. Delpeux and F. Béguin, *'Nanotubular Materials as Electrodes for Supercapacitors'*, Fuel Processing Technology, **77** (2002): p213.
39. Y.-T. Kim and T. Mitani, *'Competitive effect of carbon nanotubes oxidation on aqueous EDLC*

performance: Balancing hydrophilicity and conductivity', Journal of Power Sources, **158** (2006): p1517.

40. E. Frackowiak, *'Carbon materials for superacapcitor application'*, Physical Chemistry Chemical Physics, **9** (2007): p1774.
41. Y. Show and K. Imaizumi, *'Decrease in equivalent series resistance of electric double-layer capacitor by addition of carbon nanotube into the activated carbon electrode'*, Diamond and Related Materials, **15** (2006): p2086.
42. C.Y. Lee, H.M. Tsai, H.J. Chuang, S.Y. Li, P. Lin and T.Y. Tseng, *'Characteristics and Electrochemical Performance of Supercapacitors with Manganese Oxide-Carbon Nanotube Nanocomposite Electrodes'*, Journal of the Electrochemical Society, **152** (2005): pA716.
43. K.H. An, K.K. Jeon, J.K. Heo, S.C. Lim, D.J. Bae and Y.H. Lee, *'High-Capacitance Supercapacitor Using a Nanocomposite Electrode of Single-Walled Carbon Nanotube and Polypyrrole'*, Journal of the Electrochemical Society, **149** (2002): pA1058.
44. M.G. Deng, B.C. Yang, Y.D. Hu and B.H. Wang, Acta Physico-Chimica Sinica, **63** (2005): p1127.
45. E. Frackowiak, G. Lota and J. Pernak, *'Room-temperature phosphonium ionic liquids for supercapacitor application'*, Applied Physics Letters, **86** (2005): p164104.
46. K.S.W. Sing, D.H. Everett, R.A.W. Haul, L. Moscou, R.A. Pierotti, J. Rouquerol and T. Siemieniewska, *'Reporting physisorption data for gas/solid systems with special reference to the determination of surface area and porosity'*, Pure Applied Chemistry, **57** (1985): p603.
47. J.B. Donnet, R.C. Bansal and M.J. Wang, *'Carbon Black Science and Technology'*. 1993: Marcel Dekker, New York.
48. J.P. Zheng and T.R. Jow, *'A New Charge Storage Mechanism for Electrochemical Capacitors'*, Journal of the Electrochemical Society, **142** (1995): pL6.
49. W. Sugimoto, K. Yokoshima, Y. Murakami and Y. Takasu, *'Charge storage mechanism of nanostructured anhydrous and hydrous ruthenium based oxides'*, Electrochimca Acta, **52** (2006): p1742.
50. H.Y. Lee and J.B. Goodenough, *'Supercapacitor Behavior with KCl Electrolyte'*, Journal of Solid State Chemistry, **144** (1999): p220.
51. S.-C. Pang, M.A. Anderson and T.W. Chapman, *'Novel electrode materials for thin-film ultracapacitors: comparison of electrochemical properties of sol-gel-derived and electrodeposited manganese dioxide'*, Journal of the Electrochemical Society, **147** (2000): p444.
52. S.-C. Pang and M.A. Anderson, *'Novel electrode materials for electrochemical capacitors: Part II. Material characterization of sol-gel-derived and electrodeposited manganese dioxide thin films'*, Journal Materials Research, **15** (2000): p2096.
53. M. Toupin, T. Brousse and D. Bélanger, *'Charge Storage Mechanism of MnO_2 Electrode Used in aqueous Electrochemical Capacitor'*, Chemistry of Materials, **16** (2004): p3184.
54. X. Xie and L. Gao, *'Characterization of a manganese dioxide/carbon nanotube composite fabricated using an in situ coating method'*, Carbon, **45** (2007): p2365.
55. G.-X. Wang, B.-L. Zhang and M.-Z. Qu, *'Manganese oxide/MWNTs composite electrodes for supercapacitors'*, Solid State Ionics, **176** (2005): p1169.
56. K.-C. Liu and M.A. Anderson, *'Porous Nickel Oxide/Nickel Films for Electrochemical*

Capacitors', Journal of the Electrochemical Society, **143** (1996): p124.

57. V. Srinivasan and J.W. Weidner, *'An Electrochemical Route for Making Porous Nickel Oxide Electrochemical Capacitors'*, Journal of the Electrochemical Society, **144** (1997): pL210.
58. K.-W. Nam and K.-B. Kim, *'A Study of the Preparation of NiO_x Electrode via Electrochemical Route for Supercapacitor Applications and Their Charge Storage Mechanism'*, Journal of the Electrochemical Society, **149** (2002): pA346.
59. C.-C. Hu and C.-Y. Cheng, *'Ideally Pseudocapacitive Behavior of Amorphous Hydrous Cobalt-Nickel Oxide Prepared by Anodic Deposition'*, Electrochemical and Solid-State Letters, **5** (2002): pA43.
60. S.-Y. Wang and N.-L. Wu, *'Operating characteristics of aqueous magnetite electrochemical capacitors'*, Journal of Applied Electrochemistry, **33** (2003): p345.
61. K.R. Prasad and N. Miura, *'Electrochemical synthesis and characterization of nanostructured tin oxide for electrochemical redox supercapacitors'*, Electrochemistry Communications, **6** (2004): p849.
62. H.Y. Lee and J.B. Goodenough, *'Ideal Supercapacitor Behavior of Amorphous $V_2O_5{\cdot}nH_2O$ in Potassium Chloride (KCl) Aqueous Solution'*, Journal of Solid State Chemistry, **148** (1999): p81.
63. E. Frackowiak, V. Khomenko, K. Jurewicz, K. Lota and F. Béguin, *'Supercapacitors based on conducting polymers/nanotubes composites'*, Journal of Power Sources, **153** (2006): p413.
64. V. Gupta and N. Miura, *'High performance electrochemical supercapacitor from electrochemically synthesized nanostructured polyaniline'*, Materials Letters, **60** (2006): p1466.
65. L.Z. Fan and J. Maier, *'High-performance polypyrrole electrode materials for redox supercapacitors'*, Electrochemistry Communications, **8** (2006): p937.
66. Y. Xu, J. Wang, W. Sun and S. Wang, *'Capacitance properties of poly(3,4-ethylenedioxythiophene)/polypyrrole composites'*, Journal of Power Sources, **159** (2006): p370.
67. J. Dupont and P.A.Z. Suarez, *'Physico-chemical processes in imidazolium ionic liquids'*, Physical Chemistry Chemical Physics, **8** (2006): p2441.
68. J. Wei, *The development of manganese oxide electrodes for electrochemical supercapacitors.* 2007, McMaster University: Hamilton. p. 109.
69. I. Zhitomirsky, *'Cathodic electrodeposition of ceramic and organoceramic materials. Fundamental aspects'*, Advances in Colloid and Interface Science, **97** (2002): p279.
70. I. Zhitomirsky, *'Electrophoretic and electrolytic deposition of ceramic coatings on carbon fibers'*, Journal of the European Ceramic Society, **18** (1998): p849.
71. I. Zhitomirsky, *'Ceramic Films Using Cathodic Electrodeposition'*, JOM-e Journal of the Minerals, Metals and Materials Society, **52** (2000): http://www.tms/org/pubs/journals/JOM/0001/Zhitomirsky/Zhitomirsky-0001.html.
72. R. Damodaran and B.M. Moudgil, *'Electrophoretic Deposition of Calcium Phosphates from Non-Aqueous Media'*, Colloids and Surfaces A: Physicochemical and Engineering Aspects, **80** (1993): p191.
73. C.-C. Hu and T.-W. Tsou, *'Ideal capacitive behavior of hydrous manganese oxide prepared by anodic deposition'*, Electrochemistry Communications, **4** (2002): p105.
74. J.-K. Chang and W.-T. Tsai, *'Material Characterization and Electrochemical Performance of*

Hydrous Manganese Oxide Electrodes for Use in Electrochemical Pseudocapacitors', Journal of the Electrochemical Society, **150** (2003): pA1333.

75. Y.-S. Chen, C.-C. Hu and Y.-T. Wu, *'Capacitive and textural characteristics of manganese oxide prepared by anodic deposition: effects of manganese precursors and oxide thickness'*, Journal of Solid State Chemistry, **8** (2004): p467.
76. N. Nagarajan, H. Humadi and I. Zhitomirsky, *'Cathodic electrodepostion of MnO_x films for electrochemical supercapacitors'*, Electrochimica Acta, **51** (2006): p3039.
77. J. Wei, N. Nagarajan and I. Zhitomirsky, *'Manganese oxide films for electrochemical supercapacitors'*, Journal of Materials Processing Technology, **186** (2007): p356.
78. I. Zhitomirsky, M. Cheong and J. Wei, *'The cathodic electrodeposition of manganese oxide films for electrochemical supercapacitors'*, JOM Journal of the Minerals, Metals and Materials Society, (2007): p66.
79. M. Cheong and I. Zhitomirsky, *'Electrophoretic Deposition of Manganese Oxide Films'*, Surface Engineering, in press.
80. C.-Y. Chen, Y.-R. Lyu, C.-Y. Su, H.-M. Lin and C.-K. Lin, *'Characterization of spray pyrolyzed manganese oxide powders deposited by electrophoretic deposition technique'*, Surface & Coating Technology, **202** (2007): p1277.
81. C.-K. Lin, K.-H. Chuang, C.-Y. Lin, C.-Y. Tsay and C.-Y. Chen, *'Manganese oxide films prepared by sol-gel process for supercapacitor applicationManganese oxide films prepared by sol-gel process for supercapacitor application'*, Surface & Coatings Technology, **202** (2007): p1272.
82. K.-W. Nam and K.-B. Kim, *'Manganese oxide film electrodes prepared by electrostatic spray deposition for electrochemical capacitors'*, Journal of the Electrochemical Society, **153** (2006): pA81.
83. Y. Dai, K. Wang, J. Zhao and J. Xie, *'Manganese oxide film electrodes prepared by electrostatic spray deposition for electrochemical capacitors from the $KMnO_4$ solution'*, Journal of Power Sources, **161** (2006): p737.
84. B. Djurfors, J.N. Broughton, M.J. Brett and D.G. Ivey, *'Microstructural characterization of porous manganese thin films for electrochemical supercapacitor applications'*, Journal of Materials Science, **38** (2003): p4817.
85. T. Brousse, P.-L. Taberna, O. Crosnier, R. Dugas, P. Guillemet, Y. Scudeller, Y. Zhou, F. Favier, D. Bélanger and P. Simon, *'Long-term cycling behavior of asymmetric activated carbon/MnO_2 aqueous electrochemical supercapacitor'*, **173** (2007): p633.
86. S. Ching, D.J. Petrovay, M.L. Jorgensen and S.L. Suib, *'Sol-gel synthesis of layered birnessite-type manganese oxides'*, Inorganic Chemistry, **36** (1997): p883.
87. J. Moon, M. Awano, H. Takagi and Y. Fujishiro, *'Synthesis of nanocrystalline manganese oxide powders: Influence of hydrogen peroxide on particle characteristics'*, Journal of Materials Research, **14** (1999): p4594.
88. Q.M. Yang, V.A. Ettel, J. Babjak, D.K. Charles and M.A. Mosoiu, *'Pasted $Ni(OH)_2$ Electrodes Using Ni Powders for High-Drain-Rate, Ni-Based Batteries'*, Journal of the Electrochemical Society, **150** (2003): pA543.
89. Y. Yu, C.-H. Chen, J.-L. Shui and S. Xie, *'Nickel-Foam-Supported Reticular CoO-Li_2O*

Composite Anode Materials for Lithium Ion Batteries', Angewandte Chemie International Edition, **44** (2005): p7085.

90. A. Yuan and Q. Zhang, *'A novel hybrid manganese dioxide/activated carbon supercapacitor using lithium hydroxide electrolyte'*, Electrochemistry Communications, **8** (2006): p1173.
91. Y.-G. Wang, L. Yu and Y.-Y. Xia, *'Electrochemical capacitance performance of hybrid supercapacitors based on $Ni(OH)_2$/Carbon nanotube composites and activated carbon'*, Journal of the Electrochemical Society, **153** (2006): pA743.
92. R.K. Sharma, H.-S. Oh, Y.-G. Shul and H. Kim, *'Carbon-supported, nano-structured, manganese oxide composite electrode for electrochemical supercapacitor'*, Journal of Power Sources, **173** (2007): p1024.
93. J.Y. Lee, K. Liang, K.H. An and Y.H. Lee, *'Nickel oxide/carbon nanotubes nanocomposite for electrochemical capacitance'*, **150** (2005): p153.
94. E. Raymundo-Piñero, V. Khomenko, E. Frackowiak and F. Béguin, *'Performance of manganese oxide/CNTs composites as electrode materials for electrochemical capacitors'*, Journal of the Electrochemical Society, **152** (2005): pA229.
95. V.I. Chani, Q. Yang, D.S. Wilkinson and G.C. Weatherly, *'Effect of substrate pre-coating on adhesion of sintered nickel plaques for electrode application in rechargeable batteries'*, Journal of Power Sources, **142** (2005): p370.
96. E. Cormier, E.B. Wasmund, L.V. Renny, Q.M. Yang and D. Charles, *'A new powder morphology for making high-porosity nickel structures'*, Journal of Power Sources, **171** (2007): p999.
97. B.E. Conway and W.G. Pell, *'Power limitations of supercapacitor operation associated with resistance and capacitance distribution in porous electrode devices'*, Journal of Power Sources, **105** (2002): p169.
98. W.G. Pell, A. Zolfaghari and B.E. Conway, *'Capacitance of the double-layer at polycrystalline Pt electrodes bearing a surface-oxide film'*, Journal of Electroanalytical Chemistry, **532** (2002): p13.
99. S. Mitra, K.S. Lokesh and S. Sampath, *'Exfoliated graphite-ruthenium oxide composite electrodes for electrochemical supercapacitors'*, Journal of Power Sources, **185** (2008): p1544.
100. I. Santacruz, C.A. Gutiérrez, M.I. Nieto and R. Moreno, *'Application of alginate gelation to aqueous tape casting technology'*, Materials Research Bulletin, **37** (2002): p671.
101. P.M. Biesheuvel and H. Verweij, *'Theory of cast formation in electrophoretic deposition'*, Journal of the American Ceramic Society, **82** (1999): p1451.
102. H. Ohshima, *'Electrophoretic mobility of a cylindrical colloidal particle in a salt-free medium'*, Journal of Colloid and Interface Science, **255** (2002): p202.
103. M.S. Kumar, T.H. Kim, S.H. Lee, S.M. Song, J.W. Yang, K.S. Nahm and E.-K. Suh, *'Influence of electric field type on the assembly of single walled carbon nanotubes'*, Chemical Physics Letters, **383** (2004): p235.
104. S.-F. Chin, S.-C. Pang and M.A. Anderson, *'Material and Electrochemical Characterization of Tetrapropylammonium Manganese Oxide Thin Films as Novel Electrode Materials for Electrochemical Capacitors'*, Journal of the Electrochemical Society, **149** (2002): pA379.
105. S.C. Tjong, G.D. Liang and S.P. Bao, *'Electrical behavior of polypropylene/multiwalled carbon nanotube nanocomposites with low percolation threshold'*, Scripta Materialia, **57** (2007): p461.

106. Z. Yu, Y. Huang, C. Wang and S. Ouyang, *'A novel gel tape casting process based on gelation of sodium alginate'*, **30** (2004): p503.
107. I. Zhitomirsky and A. Petric, *'Electrophoretic deposition of electrolyte materials for solid oxide fuel cells'*, Journal of Materials Science, **39** (2004): p825.
108. A.R. Boccaccini and I. Zhitomirsky, *'Application of electrophoretic and electrolytic deposition techniques in ceramics processing'*, Current Opinion in Solid State and Materials Science, **6** (2002): p251.
109. G.M. Jacob and I. Zhitomirsky, *'Microstructure and properties of manganese dioxide films prepared by electrodeposition'*, Applied Surface Science, **254** (2008): p6671.